

Study of Cluster Ions by Mass Spectrometry and Optical Spectroscopy

A THESIS

submitted for the Award of Ph. D. degree of

MOHANLAL SUKHADIA UNIVERSITY

in the

Faculty of Science

by

Arvind Kumar Saxena



Under the Supervision of

Bhas Bapat, Associate Professor

Physical Research Laboratory, Ahmedabad, INDIA

DEPARTMENT OF PHYSICS

FACULTY OF SCIENCE

MOHANLAL SUKHADIA UNIVERSITY

UDAIPUR

2013

To

My Parents

and

My Elder Brother

Late Krishna Kumar Saxena

DECLARATION

*I, Mr. Arvind Kumar Saxena, S/O Late Shyam Swaroop Saxena, permanent resident of Mohalla mohammad zai, H. No. 521, Shahjahanpur (U.P.)-242001, hereby declare that the research work incorporated in the present thesis entitled “**Study of cluster ions by Mass spectrometry and optical spectroscopy**” is my own work and is original. This work (in part or in full) has not been submitted to any University for the award of a Degree or a Diploma. I have properly acknowledged the material collected from secondary sources wherever required. I solely own the responsibility for the originality of the entire content.*

Date:

(Arvind Kumar Saxena)

CERTIFICATE

I feel great pleasure in certifying the thesis entitled “**Study of Cluster Ions by Mass Spectrometry and Optical Spectroscopy**” by Arvind Kumar Saxena under my guidance. He has completed the following requirements as per Ph.D. regulations of the University

- (a) Course work as per the university rules.
- (b) Residential requirements of the university.
- (c) Regularly submitted six monthly progress report.
- (c) Presented his work in the departmental committee.
- (d) Published/accepted minimum of one research paper in a referred research journal.

I am satisfied with the analysis of data, interpretation of results and conclusions drawn.

I recommend submission of the thesis.

Date: 2013

Bhas Bapat
(Thesis Supervisor)
Associate Professor
Physical Research Laboratory
Ahmedabad, India.

*Countersigned by
Head of the Department*

Acknowledgments

My thesis would not have been possible without the help of several persons from different aspects such as financial support, scientific discussions, setting up and performing experiments, and emotional support. During the time of my PhD studies in Physical Research Laboratory (PRL), plenty of ups and downs occurred in my academic carrier. But this is all past, the time has come when I must thank all the persons who have provided me their affection, care and helped me in my academic carrier when it was much needed.

It has been a great privilege to spend several years in Physical Research Laboratory, a reputed institute, where I was given an extremely academically competitive yet homely atmosphere throughout my entire PhD tenure. All the members of Physical Research Laboratory, under the esteemed leadership of the Director, Prof J. N. Goswami, have carved a niche in the various emerging fields of science and technology and all of them will always remain like a family member to me.

First and foremost, I am deeply indebted and grateful to my supervisor Prof Bhas Bapat, for being so inspirational and supportive to me. I am grateful to him for his thorough and detailed revision of my work. He nurtured a great sense of freedom in me and allowed it to flourish to the highest possible extent. Apart from being my PhD mentor, I must thank him for the stimulating broad discussions that not only helped me to understand the subject but also enlightened me on the basic values and ethics in scientific activities. He brought confidence in me by showing his trust in my abilities for leading the experiments, to exchange ideas during scientific discussions, and writing the manuscripts. He walked with me during the ups and downs in developing the experimental setups. I must thank him for supporting, guiding and motivating me at adverse stages of my life during the PRL stay. I hope that I can in turn pass on the research values that he has given to me.

I would also like to thank Prof K. P. Subramanian for providing encouraging and constructive feedback. Apart from fruitful scientific discussions, he was always present for me to support emotionally. His simplistic way of teaching basic ideas of experiments and science reminds me my college teachers, his help in this aspect would be unforgettable to me. His thorough help, with his insightful thought on expressing scientific work, is gloriously reflected in my thesis.

My sincere and heartfelt gratitude goes to Prof Ajai Kumar, Institute of Plasma Research (IPR), for allowing me to use the facilities available in their laboratory.

I must thank him for encouraging as well as helping me during experiments in IPR. In this context, I would also like to thank Dr Rajesh Kumar Singh, IPR, for fruitful scientific discussions and his help during experiments in IPR. My heartfelt thanks goes to him for showing his patience to listen my ideas, appreciating as well as modifying them. He was always there for me to help scientifically as well as emotionally. I would like to thank Plasma Science Society of India (PSSI) for providing me partial financial support during experiments in IPR. I would like to thank Vishnu for helping in setting up the synchronization of different pulses.

My debt of gratitude also goes to Prof Rama Shankar, Banaras Hindu University, who provided me necessary advices which became useful to proceed through my research.

My special thanks go to the academic committee for thoroughly reviewing my work. I would also like to express my gratitude to faculty members in the Space and Atmospheric Science division, Prof D. Pallamraju, Prof Shyam Lal, Prof R. Sekar, Prof Harish Chandra, Prof S. Ramachandran, Prof S. A. Haidar, Dr Som Sharma, Dr Lokesh Sahu, Dr Smitha Thampi, Dr Dibyendu Chkarabarty for taking part in stimulating discussions and providing an outstanding flavor of doing research. My thanks are due to T. A. Rajesh (Rajesh bhai), R. P. Bhai, Sunil Bhai and S. Venkataramani for encouraging me. Along with that I would like to thank faculty members of PRL, Prof Utpal Sarkar, Prof N. Mahajan, Prof Joshipura, Prof D. Angom, Prof Prashanta Panigrahi, Prof K. K. Marhas, Dr R. P. Singh, Dr Gautam Samanta and Dr Bhushit Vaishnav. Their guidance and support has served me well and I owe them my heartfelt appreciation.

I would like to thank V. K. Lodha and I. A. Prajapati (Ishwar Bhai) for providing me untiring technical help in developing the experimental set-ups in our laboratory. My heartfelt gratitude goes to my lab-mates, Rajesh Kushwaha, Bhavesh Patel, Amrendra and Koushik for helping me and for making my stay comfortable. I can not proceed further without giving my heartfelt thank to S. B. Banerjee (Swaroop Da) and Prashant Kumar, who are more than a staff to me. They always provided me their help– personally as well as professionally.

Research life in the field of instrumentations is never possible without the help and support of persons who can make the essential parts of Instruments. In this aspect, I would like to thank all staff members of PRL Workshop including G. P. Ubale, H. R. Vaghela, Rajesh Kaila, Vishnu Patel and Bipin Kaila.

I thank all the present and past members of the Computer Center, PRL Library, Administration and Canteen. I thankfully acknowledge the help from all members of computer center Jigar Bhai, Tejas Bhai, Mishra ji and Alok Bhai. I thank Nishtha madam, Pragya, Alam and other library staff members for their cooperation and facilitating me with the required books and journals. Thanks are due to Parul Ben, Pauline madam, Priti madam, Nandini madam, Jayashree madam, Ranganathan sir, R. S. Gupta (Gupta ji), Mehta sir, Hota ji, Pradeep Bhai, Senthil Babu, Yadav ji and Sivadasan ji for their help in various stages. The six year journey of research in PRL would not have been possible without the help from Dispensary. I would like to give my thanks to Dr Shital Patel and Dr Sameer Dani for their co-operation and help.

I would like to thanks Anil Mishra Sir for teaching me informative concepts of physics, supporting, and motivating me. A very special gratitude goes to Shailendra Kumar Singh, Anish Parwage (Anna) and Rohit Srivastava for standing beside me in times of need and for being a pillar of strength for me all throughout. They have been like the surrogate family to me, bearing the pain of my frustrations and sharing the moments of success.

I thank my batch-mates: Ashish, Neeraj, Prashant, Srinivas, Satindar, Subrata and Tapas, Juniors: Ashim, Anirban, Apurva, Newton, Chinmay, Siddharth, Shashi, Fazlul, Shradha, Ikshu, Manu, Naveen Negi, Kuldeep, Abhay, S. R. Reddy, Daamu, Arun, Sunil, Aadhi, Monojit, Avdesh, Yashpal and Seniors: Mala, Kirpa Ram, Ra-biul, Bhaskar, Suman, Vineet, Ashok, Jitendra, Arvind and Tyagi ji for making my stay at PRL comfortable.

I would not have been possible to complete the long road of PhD without the freedom provided by my family who always stood by my side with immense support and encouragement. Words are not enough to express my gratitude towards my family members. I would like to give my heartfelt thanks to Maina for always standing beside me to share the moments of happiness as well as antagonistic situations, and for igniting a strong confidence in me. Last but not the least, life is never easy without the company of friends, I offer my sincere thanks to Arvind Kumar, Nitya, Anuj, Manish, Vimal, Rajesh, Moin, Santosh, Satyendra, Umang, Vishwapal and Bhupesh for showering me with their moral and emotional support in every step of life.

At the end, I thank all the persons who have helped me during my Ph.D. Thesis.

Abstract

The course of experiments described in thesis are focused to provide insight into the production of atomic, molecular and mixed clusters from solid and gas, and the investigation of difference in ionization mechanism of clusters subjected to high intensity photon beam. Carbon cluster sources based on sputtering and laser ablation are developed to generate a beam of carbon cluster. The formation of carbon clusters in the sooting environment of these sources is confirmed using optical emission spectroscopy (OES). It is found that the dominant mechanism for cluster formation in sputtering source is the three body collision between the carbon ejecta and Argon atoms, and in laser ablation source three body collision is sole responsible for cluster formation. The detection of clusters heavier than dimer is not possible using emission spectroscopy due to the unavailability of spectroscopic data. For this purpose, time-of-flight (TOF) mass spectrometry is adopted. The detection of heavy carbon clusters and mixed clusters of carbon and Argon is confirmed using TOF technique.

To generate clusters from gas, a pulsed nozzle source is developed. Clusters from pulsed nozzle source are ionized using IR and UV irradiation of Nd:YAG laser. Using pulsed nozzle source, Xenon clusters, Ethyl alcohol clusters and mixed clusters of Ethyl alcohol, Water vapor and Benzene are produced.

Apart from developing the cluster sources, the difference in the ionization mechanism of Xenon clusters under IR and UV irradiation is studied. Multi-photon ionization of Xenon clusters produced by pulsed nozzle source has been investigated under two different wavelength ionization (IR and UV irradiation) using TOF spectrometer. Under IR, singly charged cluster ions beyond the dimer are not formed in the mass spectra, but multiply-charged atomic ions up to charged state 5+ are present. Under UV, singly charged heavy cluster ions (upto Xe_{80}^+) are detected, but no multiply charged ions are seen in the mass spectrum. The difference in the ionization mechanism of Xenon clusters is exploited to understand the effect of cluster size on the formation of multiply charged atomic ions. The cluster size in the supersonic beam is manipulated by changing the stagnation pressure. The mean cluster ion size (under UV) shows an increasing trend with the stagnation

pressure. The mean cluster ion size is used as a proxy for neutral clusters. Mass spectra are recorded under different stagnation pressures with IR irradiation. The dependence of mean kinetic energy and mean charged state of multiply charged ions with pressure, or indirectly with the cluster size has been studied. The difference in ionization mechanism of Xenon clusters provides a tool to investigate the effect of cluster size on the ionization processes and kinematics of Xenon clusters. This study also describes the formation of multiply charged atomic ions on the basis of electron re-collision model.

Keywords: Sputtering, Laser ablation, Supersonic expansion, Optical emission spectroscopy, Time-of-flight mass spectrometry, Multiphoton ionization, Multiply charged ions.

List of Publications

1. *Optical Emission Spectroscopy of Carbon Clusters Produced in a Hollow Cathode Sputter Source*

Arvind Saxena, Prashant Kumar, Swaroop Banerjee, K. P. Subramanian and Bhas Bapat

Spectroscopy Letters, 2013 (In press).

DOI:10.1080/00387010.2013.783872

Details are discussed in Chapter 3.

2. *Dependence of ion kinetic energy and charge on cluster size in multi-photon ionisation of xenon clusters*

Arvind Saxena, Prashant Kumar, S B Banerjee, K P Subramanian, B Bapat, R K Singh and Ajai Kumar

International Journal of Mass Spectrometry, 2013 (In press).

<http://dx.doi.org/10.1016/j.ijms.2013.09.002>

Details are discussed in Chapters 4 and 5.

Contents

Acknowledgments	i
Abstract	iv
1 Introduction	1
1.1 An overview	1
1.2 Issues addressed in the present work	3
1.3 Outline of the thesis	4
2 Cluster production techniques	5
2.1 Breakdown-based methods	5
2.2 Aggregation-based methods	11
3 Optical emission spectroscopy of carbon clusters	18
3.1 Optical emission spectroscopy	18
3.2 OES investigation of sputtering source	20
3.3 OES investigation of laser ablation source	26
4 Mass spectrometric study of clusters	30
4.1 Time-of-Flight (TOF) Mass Spectrometry	30
4.2 Graphite sputtering source	38
4.3 Clusters from pulsed nozzle source	39
4.4 Molecular and mixed clusters from pulsed nozzle	46
5 Multiply charged ion formation in MPI of Xenon clusters	49
5.1 IR irradiation: Multiple ionization	49

5.2	Characteristics of atomic ions resulting from MPI of clusters	52
6	Summary and future prospects	57
6.1	Summary	57
6.2	Future prospects	58
	Bibliography	60

Chapter 1

Introduction

1.1 An overview

Atomic or molecular clusters are aggregation of a few to million number of atoms or molecules held together by a binding force. Depending upon the bonding between atoms in a cluster they are classified into four categories such as ionic clusters, covalent clusters, metallic clusters and van der Waals clusters. Atomic and molecular clusters are often called a new phase of matter since they exhibit properties which are neither those of the corresponding bulk nor those of their isolated constituents. This is due to their large value of number of surface atoms to volume atoms ratio.

Among other clusters, carbon clusters play an important role in many branches of science. Neutral carbon clusters present in the atmospheric soot plays an important role in the occurrence of heterophase chemical reactions between gas molecules. From small clusters to large clusters, (such as C_{60}), carbon clusters provide a good tool to study how material properties evolve. Small carbon clusters play an important role in astrophysics and combustion [1]. They are expected to play an important role in the formation, mechanism and properties of cosmic dust [2]. There is a renewed interest in cluster science due to applications in nanotechnology [2]. Another branch where clusters play a significant role is in heterophase reactions, such as their use as catalyst in chemical industry. The collision of a cluster with atoms or molecules may lead to the adsorption of atoms onto the cluster resulting in the formation of a mixed cluster [3].

The size distribution of large neutral clusters cannot be determined experimentally without ionizing them. The general schemes for the ionization of clusters are CW UV ionization, charged particle impact ionization and multiphoton ionization (MPI) using high power lasers. Due to poor duty cycles of pulsed cluster sources, CW UV ionization is generally not used. High energy charged particle impact ionization of weakly bound van der Waals clusters leads to the fragmentation of clusters. For the production of singly charged cluster ions, MPI of clusters is generally used in the mass spectrometric measurements. In MPI scheme, depending upon the wavelength various ionization channels in clusters are observed.

The interaction of high intensity photon beam with a cluster is different compared to constituent atom or molecule. It has been found in earlier experiments that the energy coupling between a target and a short pulse laser is more efficient in case of a cluster target as compared to an atomic target [4, 5], Ions with kinetic energy 1 MeV has been observed by Ditmire et al. [6, 7] in the ionization of Xe clusters and formation of multi-keV electron with energies up to 5 keV was observed by Mcpherson et al. in ionization of Xe clusters [5]. The interaction of a photon beam with clusters may also lead to the formation of singly charged cluster ions and multiply charged atomic ions. The ion distribution in such experiments depends upon the power density and wavelength of laser beam [8–10]. The production of multiply charged ions using highly intense ($10^{15} - 10^{19} \text{ Wcm}^{-2}$) ultrashort laser pulses has been studied extensively. At such high intensities, heavy cluster ions dissociate to generate atomic ions and thus singly charged heavy cluster ions are not observed in the mass spectrum. However at moderate intensities ($10^9 - 10^{11} \text{ Wcm}^{-2}$), largest Xenon cluster ion of size 16 was reported by a Luo et al. [8]. The size of neutral clusters play an important role in the formation of ion distribution. It was found that the formation of highly charged atomic ions depends on the size of the neutral clusters [8, 10–12].

1.2 Issues addressed in the present work

The central theme of the thesis is the development of cluster sources to generate atomic, molecular and mixed clusters, and to study the interaction of clusters with atoms and high intensity photon beam. The primary step for the investigations of cluster-atom and cluster-intense photon beam interaction is the development of experimental setups for the production and detection of clusters. To generate a cluster beam from solid as well as from gas, development of cluster sources is essential.

The interaction of carbon clusters with atoms or molecules may lead to several processes, atoms may get adsorbed onto cluster leading to the formation of mixed cluster or atoms may carry the excess energy away from cluster leading to cooling and formation of heavy cluster. In presence of UV radiation, molecules adsorbed onto the surface of a carbon cluster may initiate a chemical reaction. The study of such complex heterophase reactions on carbon clusters are not well understood and demand more attention for the experimental as well as theoretical developments. The primary step in this direction would be the development of cluster source to produce a beam of carbon cluster. In the present thesis, development of carbon cluster source is discussed. Optical emission spectroscopy and time-of-flight mass spectrometry techniques are used to detect the carbon clusters.

The interaction of clusters with highly intense photon beam may lead to the formation of multiply charged ions and singly charged cluster ions. The cluster size plays a crucial role in the formation of multiply charged ions. The cluster size is generally estimated on the basis of the Hagen's theory [13]. In the present thesis, ionization mechanism of Xenon clusters subjected to IR and UV irradiation of ns pulsed Nd:YAG laser has been studied. The dependence of kinetic energy and charge state of multiply charged atomic ions on the cluster size has been investigated and presented in the thesis.

In brief, the following investigations are presented in thesis:

- Optical emission spectroscopic study of carbon soot for the formation of carbon clusters
- Production and detection of carbon clusters, Xenon clusters, Ethyl alcohol

clusters, mixed clusters composed of carbon and Argon, and Ethyl alcohol, Benzene and Water vapor.

- Investigation on the interaction of Xenon clusters with IR and UV irradiation of Nd:YAG laser
- Dependence of mean kinetic energy and charge state of multiply charged ions on the cluster size.

1.3 Outline of the thesis

The thesis has been organized into seven chapters and the outline of thesis is as follows. Chapter 1 gives the introduction of the thesis. Chapter 2 provides a brief detail of methods for the cluster production from solid as well as gas target. The cluster sources developed on these methods are also discussed in detail. Chapter 3, 4 and 5 include results from the optical emission spectroscopy and mass spectrometry of clusters. In Chapter 3, the optical emission spectroscopic technique used for the detection of carbon clusters and the emission spectroscopic investigation of carbon cluster sources are discussed. It contains discussions on the interaction of the energetic carbon ejecta with the ambient Argon gas as well as the effect of the experimental parameters of cluster source on the carbon cluster formation. Chapter 4 describes the time-of-flight mass spectrometric technique used for the detection of heavy cluster ions. Outcomes from the mass spectrometric detection of atomic, molecular and mixed cluster are discussed in this chapter. Chapter 5 includes the significant outcomes from the multiphoton ionization of Xe clusters exposed to ns pulsed IR irradiation. The formation of multiply charged atomic ions has been briefly discussed on the basis of electron re-collision model. Chapter 7 briefly summarizes the outcomes from the thesis. It also briefly outlines the possibilities for further study .

Chapter 2

Cluster production techniques

2.1 Breakdown-based methods

Clusters can be generated from solid by breaking it into miniature fragments. Fragmentation of solid can be achieved by imparting adequate energy, greater than the binding energy of atoms in solid. In order to fracture a solid surface and to produce clusters, there are basically two methods, namely, sputtering and laser ablation.

In general, ions can be either from an accelerator [14–16] or from the plasma generated in low pressure ambient [17, 18]. The cluster source based on ion bombardment is known as hollow cathode sputtering source. Plasma ion bombardment is a very simple technique as compared to the ion bombardment from an accelerator.

The ion bombardment technique is generally employed for either generating ions or for thin film deposition. For producing a beam of neutral clusters, laser ablation technique accompanied by supersonic expansion is generally used. In this method, intense laser pulse is focused on to a target. The ejecta in plasma plume is cooled by a synchronized high pressure gas pulse.

Plasma ion sputtering

The first experimental observation of sputtering by low energy ion bombardment was by Wehner et al. in 1953 [19]. In D.C. discharge plasma ion sputtering, an inert gas is passed between two electrodes. Cathode is made from the material

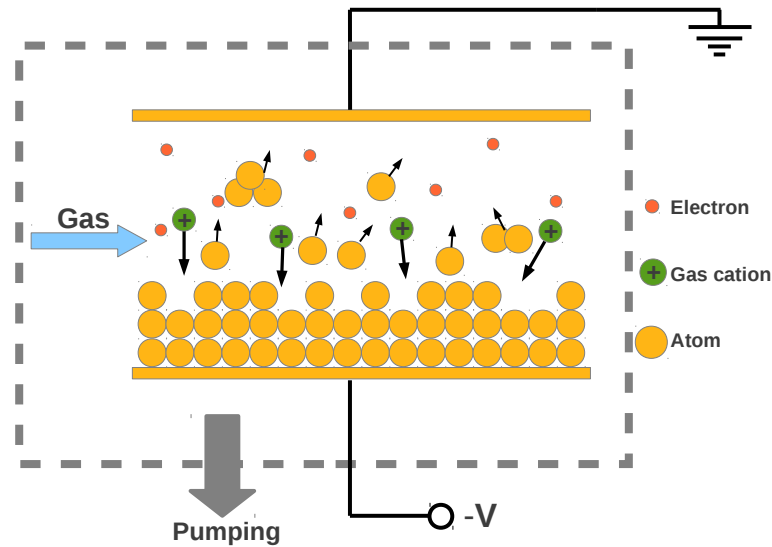


Figure 2.1: Schematic diagram of D.C. discharge sputtering source. The dashed line represents the vacuum enclosure. Gas enters between the electrodes made from the material of interest. Due to the applied field, breakdown of gas occurs resulting in the formation of plasma. Cation from the plasma strikes the cathode and atoms, molecules and clusters are ejected from the surface.

of interest and is negatively biased. The bombardment of energetic cations on the cathode surface results in the ejection of energetic atoms, electrons and clusters. This ejection process from the solid surface is known as sputtering. The energy of cations plays a crucial role in sputtering. The minimum energy required for sputtering depends on the surface binding energy of solid. The number of atoms sputtered with respect to an ion bombardment is generally known as sputter yield. A schematic diagram for D.C. discharge sputtering is shown in Figure (2.1).

The sputtering source generates a mixture of neutral and ionized clusters [18, 20–22]. For producing a beam of neutral clusters, cooling of sputtered species as well as a jet formation is essential. Sputtering source is generally used either for thin film deposition or for cluster ion production. To generate a beam of neutral clusters, modifications in the design of sputtering source is required.

Hollow cathode sputtering source

Hollow cathode sputtering sources are considered to be very efficient sources for creating the sooting environment which can lead to the formation of carbon clusters

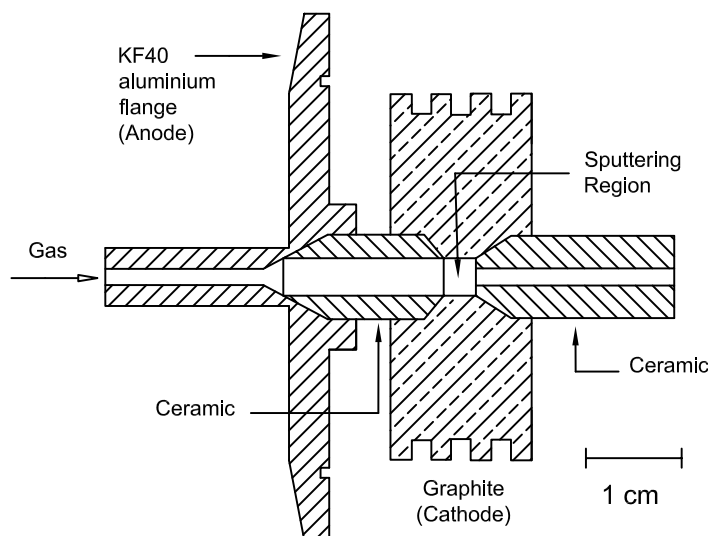


Figure 2.2: Schematic diagram of the hollow cathode carbon cluster source. The sputtering region is 4 mm in length and 4 mm in diameter; the figure is approximately to scale. The source resides entirely in vacuum, the vacuum coupling being made via a KF-40 flange which serves as the (grounded) anode and has a provision for admitting gas. High voltage connection to the cathode is made via an auxiliary electrical feedthrough.

[18, 23]. The sputtering sources are bulky in size and they are used for thin film deposition [24, 25], spectroscopic study of the soot [26] and production of ions [18]. In order to generate a beam of neutral clusters, significant modifications are needed. We have implemented the modifications in the design of cluster source which makes it more versatile, in terms of beam production, than other sources [17, 18].

A schematic diagram of the carbon cluster source is shown in Figure (2.2). The cluster source is made from graphite and is in the form of a cylinder with an axial cavity of 4 mm length and 4 mm diameter. Graphite is kept at a negative voltage of 0.5–1.2 kV and works as a cathode. The cathode is axially coupled via a ceramic spacer to an aluminium flange. It is grounded and acts as an anode. An ambient Argon atmosphere at a pressure of 1.0–3.5 mbar, monitored using a Pirani gauge, is maintained within the cavity to ensure a stable discharge. Differential pumping is maintained in the source chamber. The cluster beam is extracted by a skimmer of 1.0 mm aperture. The source chamber is pumped by a turbo pump (210 l s^{-1}), backed by a rotary and Roots pump. The lowest pressure obtained in the source chamber is 5×10^{-6} mbar.

The source is compact (25 mm in length and 38 mm in diameter) compared to



Figure 2.3: Photograph of the compact hollow cathode carbon cluster source.

other sources, such as, a hollow cathode source of dimensions 60 mm in length and 60 mm in diameter was developed by Shoaib et al. [18] for generating carbon ions and for performing emission spectroscopy of carbon soot. Our source has a large outer surface area which permits rapid heat dissipation. The gas consumption is low since the gas is admitted as a jet at a pressure of 1.0–3.5 mbar via a 4 mm aperture close to the sputtering region. The coupling of source with a vacuum chamber is very easy as source is mounted on a KF-40 flange. The ceramic nozzles are designed to maintain a jet of gas carrying the sputtered particles and clusters. The diameter of the first nozzle is large while the diameter of the second nozzle (right to source) is small and has a long channel. The long channel support enhanced three body collisions between the ejecta and Argon atoms before the departure from the nozzle exit. A jet of particles is released at the exit of second nozzle. A carbon spot, 3 mm in diameter, is observed on a holder placed at 100 mm from the plasma region.

I-V Characteristic of sputtering source

The variation of voltage drop (V_{drop}) across the plasma with the discharge current (I_{dis}) as well as with the Argon gas pressure (P) is studied. The relation between voltage drop and discharge, voltage drop and Argon gas pressure is shown in Figure

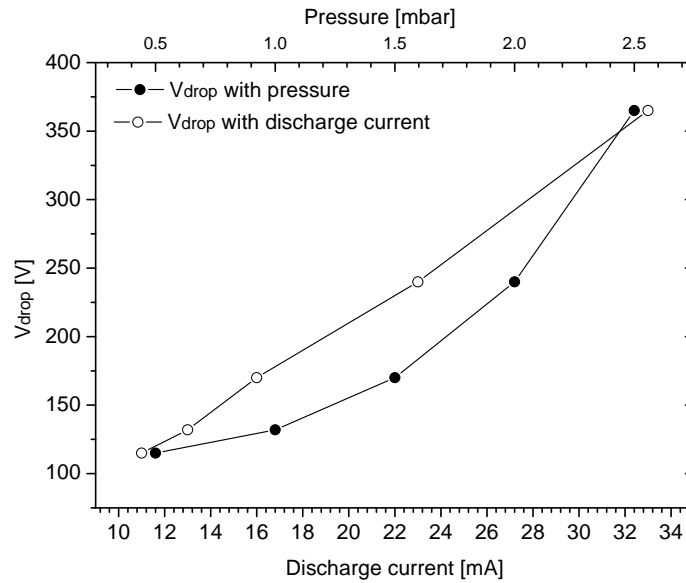


Figure 2.4: Variation of voltage drop with discharge current (open circle) and Argon gas pressure (filled circle).

2.4. It is found that an increase in pressure and discharge current lead to an increase in the voltage drop across the plasma.

Laser ablation of solids

The method of breaking a solid surface with high power density laser beam is very popular for thin film depositions, material characterization, cluster production, micro-structure generation, spectroscopy and mass spectrometry. The first evaporation experiment involving a gold target irradiated by a Q-switched ruby laser was performed by Levine et al. in 1968 [27]. Since then this method is used extensively by many groups [27–30]. In laser ablation, the electromagnetic energy of incident radiation on solid leads to the melting, vaporization and formation of hot plasma plume from the surface. The plasma plume consists of atoms, molecules, clusters, cations, anions, electrons and photons. The onset value of laser fluence for ablation depends on material properties (metal, semiconductor or insulator).

Laser ablation method has been used to generate large clusters from solid surface [31–33]. Laser ablation provides freedom to manipulate the cluster size within large limits. However in order to produce a beam of neutral clusters, the cooling of

hot ejecta in the plasma plume is essential. For this purpose, a combination of laser ablation and high pressure gas is widely used by many groups [31–35].

Laser ablation source

Laser ablation source accompanied by high pressure gas expansion is a very popular technique for producing clusters from solid. The first laser vaporization source was developed in 1981 by R. E. Smalley and his co-workers at Rice University [36]. The versatility of Smalley source has proven to be quite remarkable. For the efficient cooling of plasma plume, a channel is often provided in the laser ablation source. The channel brings gas at the point of ablation. The Smalley group proposed an improved design of the ablation source for the cluster formation. They introduced a waiting room for the ablated species. In their design, there is a section of reduced channel diameter followed by an extended diameter exit. The gas undergoes rapid collisions with the plume ejecta before exit from the channel. Thus rate of three body collisions is higher with this design leading to production of larger clusters. The discovery of C_{60} was using this source by Smalley et al. [31]. It was found that the deposition of ablated species inside the channel of cluster source may affect the cluster formation [32]. To prevent the degradation of cluster formation, de Heer et al. proposed an improved and compact design in which they introduced a cavity for the plume confinement. The channel was designed so that gas turbulence prevails leading to enormous collisions between ejecta and gas and formation of clusters [32].

Owing to the simplicity and advantage of rapid collisions for cluster formation in cluster source by de Heer et al. , a cluster source based on this design is developed in our lab. The schematic diagram of ablation source is shown in Figure (2.5). In the present cluster source, excimer laser pulses (248 nm, 20 ns, 10–50 Hz, upto 400 mJ) are focused using a lens of 50 cm focal length of intensity 10^9 W cm^{-2} on to a rotating graphite disk. The graphite disk is rotated using a rotary feed-through to expose a fresh area for each incoming laser pulse. This prevents the surface hardening problem and deep drilling on the disk surface. The interaction of nanosecond pulse with graphite leads to the formation of plasma plume. The carbon

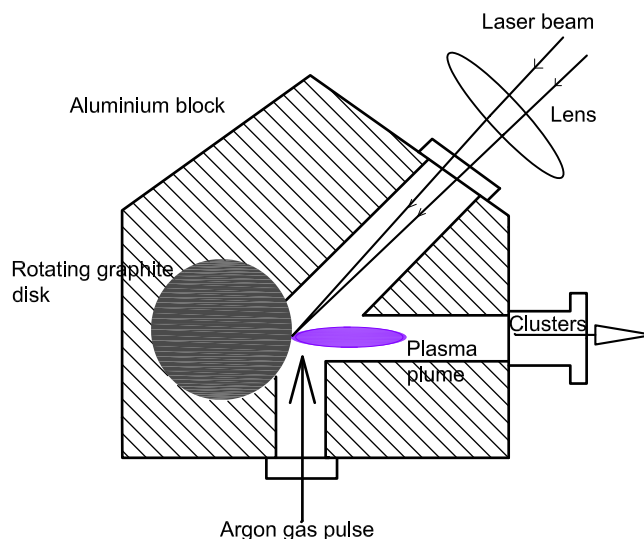


Figure 2.5: Schematic diagram of laser ablation source coupled with gas expansion. Excimer laser pulses are focused on to a rotating graphite disk. Ejecta in the plasma plume are cooled using high pressure Argon gas pulses ejected by a pulsed nozzle (0.5 mm diameter).

ejecta in the plasma plume are hot species and in order to generate clusters, cooling of these ejecta is essential.

For this purpose, high pressure Argon gas pulses, ejected by a pulsed nozzle (*Parker*) of 0.5 mm diameter, are synchronized with plasma plume with a certain time delay. The synchronization of gas pulse and the excimer laser pulse is such that plume is produced when the maximum of gas pulse passes the disk surface. The collisions between ablated carbon species and Argon atoms inside the channel lead to the formation of carbon clusters.

2.2 Aggregation-based methods

For generating clusters from atoms or molecules, they can be cooled down. For achieving the cooling of gas, it is expanded from a very high pressure (few atmospheres) region to a low pressure region (high vacuum) in pulsed form. The method for attaining the sufficient cooling of atomic or molecular species is the supersonic expansion of gas.

Supersonic expansion of gas

Supersonic beam is characterized by a quantity which is the ratio of average flow velocity of atoms (v) to the local speed of sound (v_s). This quantity is known as Mach number (M). For an expansion to be supersonic, M should be greater than 1.

$$M = \frac{v}{v_s} = v \sqrt{\frac{m}{\gamma RT}} \quad (2.1)$$

here v is average flow the velocity of atoms, v_s is the local speed of sound, R is gas constant, T is the temperature in the stagnation region, m is the molar mass . The maximum terminal velocity (v_{max}) of an ideal gas for an isentropic nozzle expansion can be calculated by employing first law of thermodynamics.

$$v_{max} = \sqrt{\frac{2C_p T}{m}} \quad (2.2)$$

The specific heat (C_p) at constant pressure is given as,

$$C_p = \left(\frac{\gamma}{\gamma - 1} \right) R \quad (2.3)$$

Therefore the maximum terminal velocity can be given as,

$$v_{max} = \sqrt{\frac{2RT}{m} \times \frac{\gamma}{\gamma - 1}} = v_{mp} \times \sqrt{\frac{\gamma}{\gamma - 1}} \quad (2.4)$$

where R is gas constant, T is the temperature in the stagnation region, m is the molar mass and C_p is the heat capacity at constant pressure, γ is ratio of specific heat, T is local translational temperature and v_{mp} is the most probable Maxwellian speed in the reservoir.

When atoms having mean free path λ in an enclosure expands through an aperture of diameter d in a regime $\lambda \ll d$, atoms escaping from the aperture suffer enormous collisions. A schematic diagram of supersonic expansion of gas is shown in Figure (2.6).

A pulsed nozzle with nozzle diameter d is at stagnation pressure P_0 and temper-

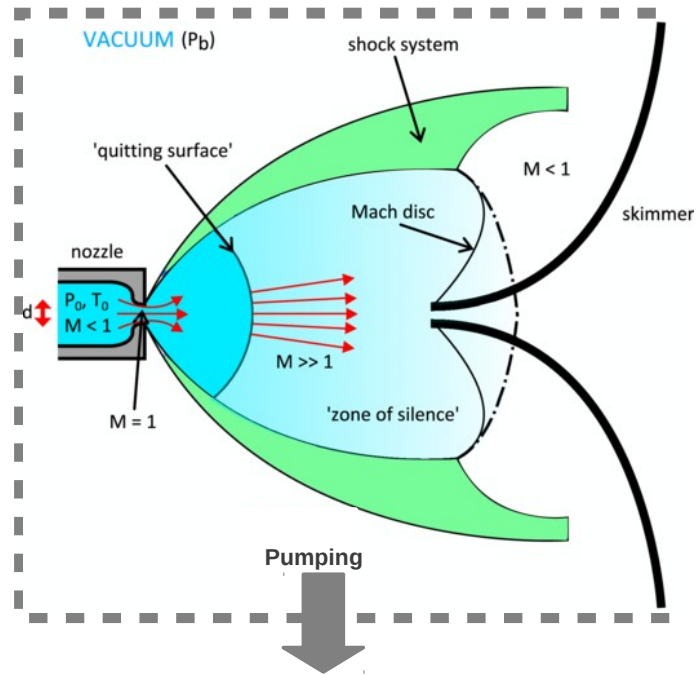


Figure 2.6: Schematic diagram of supersonic expansion of gas from a pulsed nozzle.
Source: M. Barr et al. *Meas. Sci. Technol.* **23**, 105901 (2012).

ature T_0 . It ejects gas pulses from high pressure (few atmosphere to several atmosphere) reservoir into a low background pressure (P_b) environment. The adiabatic expansion of gas triggers collision cascade between the atoms leading to cooling and cluster formation. Thus the random thermal energy of particle is converted in to directed kinetic energy.

After the ejection of gas pulse from pulsed nozzle, gas enters into a region where the velocity of atoms exceeds the local speed of sound and $M > 1$, this region is known as silence zone. The boundary of this zone is called as Mach disk.

Beyond the Mach disk location the local speed of sound overcomes the velocity of atoms and M becomes less than 1. To avoid the scattering and attenuation of cluster beam the dense core of beam must be extracted before it crosses the Mach disk. The core of beam is generally extracted by putting a skimmer before Mach disk location. The position of Mach disk depends only on the ratio of stagnation pressure to background pressure (P_0/P_b) and the nozzle diameter (d). The location of Mach disk (X_m) is given in equation 2.5.

$$X_m = 0.67d\sqrt{P_0/P_b} \quad (2.5)$$

Nozzle geometry influences the cluster formation. Cluster formation occurs in the vicinity of nozzle aperture, within few nozzle aperture distance. It was investigated experimentally that growth of cluster, in the vicinity of nozzle aperture, is influenced by different nozzle geometries, but beyond the clustering region expansion is identical for all nozzle shape [13,37]. Thus, nozzle shape has great influence on the clustering of atoms occurring close to the nozzle exit.

Cluster formation in supersonic expansion

The first observation of cluster formation was in an experiment of gas dynamics expansion of atoms conducted by Becker et al. (1956) [38]. This method has further been used by many groups to generate weakly bound clusters from different gaseous atoms or molecules [8–10, 13, 39–43]. Cluster formation in free jet expansion has led to great advancement in understanding the weakly bound ensembles of atoms or molecules. The translational cooling rely on binary collisions and total number of binary collisions during the expansion is proportional to the P_0d . For cluster formation, the primary process is the production of a dimer by condensation of monomer via three body collisions with third body carrying the excess energy. The total number of three body collisions between the atoms during the expansion is proportional to P_0^2d whereas mass throughput is proportional to P_0d^2 .

The stagnation pressure, temperature of gas, nozzle size and its geometry affect the average cluster size in a gas jet [44]. The onset of cluster formation and the average cluster size can be estimated using Hagen's parameter [13]. The Hagen parameter (Γ^*) is defined as

$$\Gamma^* = k \frac{(d/\tan\alpha)^{0.85}}{T^{2.29}} p_0 \quad (2.6)$$

Where d is the diameter of pulsed nozzle (μm), α is the half angle of expansion, p_0 is the stagnation pressure (mbar) and k is an empirical constant which depends on type of gas ($k = 5500$ for Xe, 2890 for Kr, 1650 for Ar, 185 for Ne, and 3.85 for

He [45]). Clustering begins when $\Gamma^* > 1000$ [42]. The formation of large clusters ($> 10^4$ atoms per cluster) begins when $\Gamma^* > 5 \times 10^4$ [42].

To generate clusters from atomic or molecular vapor, it is mixed with a carrier gas. The carrier gas is, generally, an inert non-condensable gas such as He or Ne [46]. Other carrier gas can also be used but in that case condensation of atoms from solution may get affected by the excess heat released from the clustering of carrier gas. The technique of vapor mixing in a carrier gas is used to generate molecular and mixed clusters. The production of mixed clusters from different gas species is studied in many experiments [47–49]. Mixed clusters are generally produced in the supersonic expansion when the interaction energy between two atoms of injected sample is not very different from the interaction energy between injected sample atom and carrier gas atom [3].

Pulsed nozzle source

A pulsed nozzle source based on the supersonic expansion of gas is developed. The schematic diagram is shown in Figure (2.7). For the pressure conditions of present pulsed nozzle source, Mach number (M) is greater than 1, it ensures the validity of supersonic expansion. In present source, high pressure (1-8 bar) gas pulses, either Argon or Xenon, are injected by a pulsed nozzle (*Parker, series 9*) of 0.5 mm nozzle diameter into a low background pressure chamber (2×10^{-6} mbar). The gas pulse duration is set to $300 \mu s$ and repetition rate at 30 Hz for all measurements. The core of cluster beam is extracted by a home made aluminium skimmer with 1.2 mm aperture. In the present setup at 3 bar of stagnation pressure, the Mach disk is located at 366 mm from the pulsed nozzle. For ensuring the absence of shock waves during the supersonic expansion in present setup, the beam is extracted by placing a skimmer at 20 mm from the pulsed valve. It was found that the positioning of skimmer far from 20 mm distance degrade the beam quality.

The pulsed valve was mounted in a six way cross chamber with a stainless steel quarter inch pipe via top ISO-63 flange. The bottom CF-63 flange is coupled to a mass spectrometer via an aluminium barrel with base serving as a gasket. The barrel accommodates a skimmer on the top face with four screws. The top ISO-63 flange

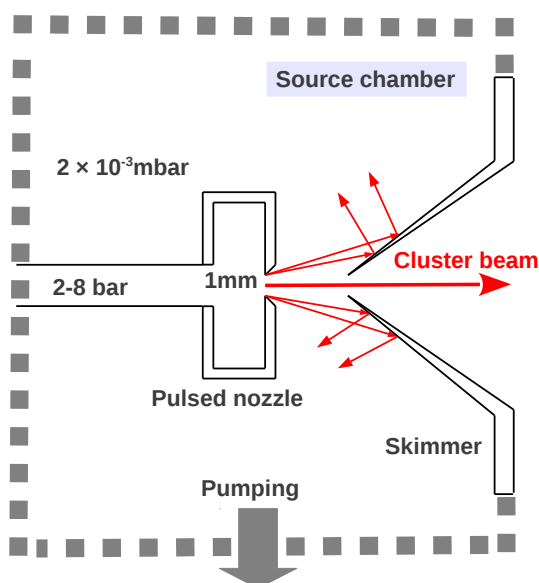


Figure 2.7: Schematic diagram of pulsed nozzle source for producing clusters from gas. Dashed line represents a vacuum enclosure. The cluster beam produced by nozzle is extracted by a skimmer of 1.2 mm aperture.

is designed in such a way that it has a central quarter inch bore for accommodating pulsed valve. A schematic diagram of ISO-63 flange accommodating pulsed nozzle is shown in Figure 2.8.

An aluminum plate with a O-ring groove and a cajon is mounted on this flange. This plate can be moved externally in x, y direction with the help of 4 screws. In the



Figure 2.8: Top view of ISO-63 flange used for mounting pulsed nozzle and to adjust it in x, y direction during the operation.

present setup, the pulsed valve mount is designed in such a way that it has a great freedom to move the pulsed valve, for aligning with the skimmer, even during the operation.

The electrical connection for pulsed valve is done by using an auxiliary KF-25 electrical feed-through. A turbo pump (230 l s^{-1}) backed by a scroll pump is incorporated for creating vacuum via a ISO-100 flange. A Penning gauge (*Edwards*) is used to monitor the pressure in source chamber. The minimum pressure achieved in the source chamber is 2×10^{-6} mbar.

With the aim of the production of a carbon cluster beam, cluster sources based on plasma ion sputtering and laser ablation are discussed. A pulsed nozzle source based on the supersonic expansion of gas is developed to generate clusters from gas. In the next two Chapters, optical emission spectroscopy and time-of-flight mass spectrometry of clusters are discussed.

Chapter 3

Optical emission spectroscopy of carbon clusters

3.1 Optical emission spectroscopy

It is discussed in Chapter 2 that sputtering source and laser ablation source are used to generate a beam of carbon clusters. In both sources, sooting environment is necessary for the production of carbon clusters. The energetic carbon ejecta in hollow cathode sputtering source and laser ablation source emit characteristic radiation during de-excitation. Due to the suitability and simplicity of optical emission spectroscopy, this technique is adopted to detect carbon clusters from the sooting environment of cluster sources.

Basic principle

The emission spectrum of a chemical element is an electromagnetic spectrum at discrete wavelengths due to the transition of electrons in an atom from higher energy level to the lower energy level. Each chemical element emits distinctive set of discrete wavelengths, and the elemental composition of the unknown sample can be easily determined by observing these wavelengths. Thus detection of the emitted radiation is a simple method for the identification of the atomic or molecular ejecta. The basic components of an emission spectrometer include monochroma-

tor or wavelength selector and a photon detector, generally, photomultiplier tube or charged couple device (CCD). The photon source in present case is hollow cathode sputtering source or laser ablation source, wavelength selector is a diffraction grating, and photon detector is a CCD.

Optical emission spectrometer

The schematic diagram of optical emission spectrometer is shown in Figure 3.1. The optical emission spectrometer set-up is used to investigate the production of carbon clusters from the glow discharge environment (hollow cathode sputtering source) and from the plasma plume environment (ablation source). The light emitted from both the cluster sources is coupled to the entrance slit of a spectrograph (*Acton Research SpectraPro 300i-P*) by a $f/2.5$ arrangement of two convex lenses of focal length 200 cm and 100 cm respectively (Figure 3.1).

The intensity of the photons is then measured by a CCD camera (*Pixis Princeton Instruments*). The spectral resolution of spectrometer is 0.3 nm. The optical emission spectrometer is calibrated with the Hg-Ar discharge lamp. The emission spectra from both sources are recorded in different experimental conditions and then analyzed.

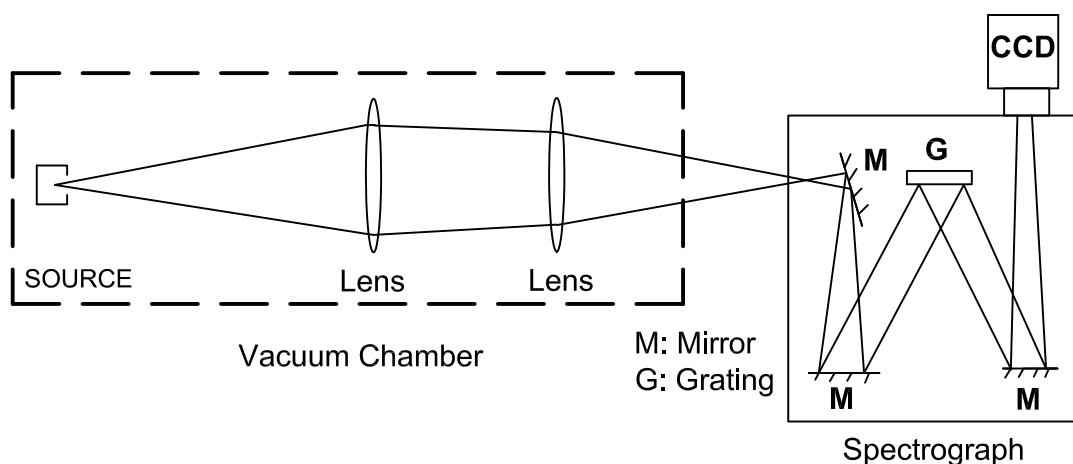


Figure 3.1: Schematic diagram of optical emission spectrograph coupled with the light of cluster source. The source and the collection optics are in vacuum.

3.2 OES investigation of sputtering source

In the present study, optical emission spectroscopy is used to detect carbon clusters in hollow cathode source. The formation of carbon clusters can be either by ejection from graphite surface due to plasma ion bombardment or by the three body collision between the atomic ejecta and ambient gas atoms. The understanding of the competitive process for the cluster production as well as control over T_{vib} with gas pressure can help to control the cluster yield by tuning the discharge parameters, such as, discharge current and gas pressure.

Emission spectra from sputtering source

The analyzed emission spectra from the sputtering source reveal the presence of C_2 Swan band, C ionic lines, Argon atomic lines and Argon ionic lines in the glow discharge environment (Figure 3.2). The spectral analysis of C_2 was first performed by William Swan in 1856 [50]. The sequences of vibrational band of C_2 covering a range in the visible spectrum are called Swan band. Swan bands are characteristic of the spectra of carbon, carbon stars, comets and of hydrocarbon fuels. The observed Swan bands in the emission spectrum of sputtering source are shown in Figure 3.3.

Variation of C_2 (0–0) band intensity with discharge current

The production of C_2 can be in two ways, direct ejection from the graphite surface or by the three body collision between the atomic ejecta and Argon atoms. We have examined these possibilities one by one. The intensity of Swan band is found to be dependent on the discharge current and the gas pressure. In other words, production of C_2 Swan band in the present sputtering source can be controlled by tuning the discharge current and the Argon gas pressure.

To observe the effect of discharge current on the intensity of 0–0 band head, emission spectra are recorded at different discharge current but at constant pressure. It is found that intensity of 0–0 band head follows a linear relation with the discharge current (Figure 3.4). The dependence of the $C_2(0-0)$ intensity on the discharge current (constant Argon pressure) is not surprising, as an increase in the discharge

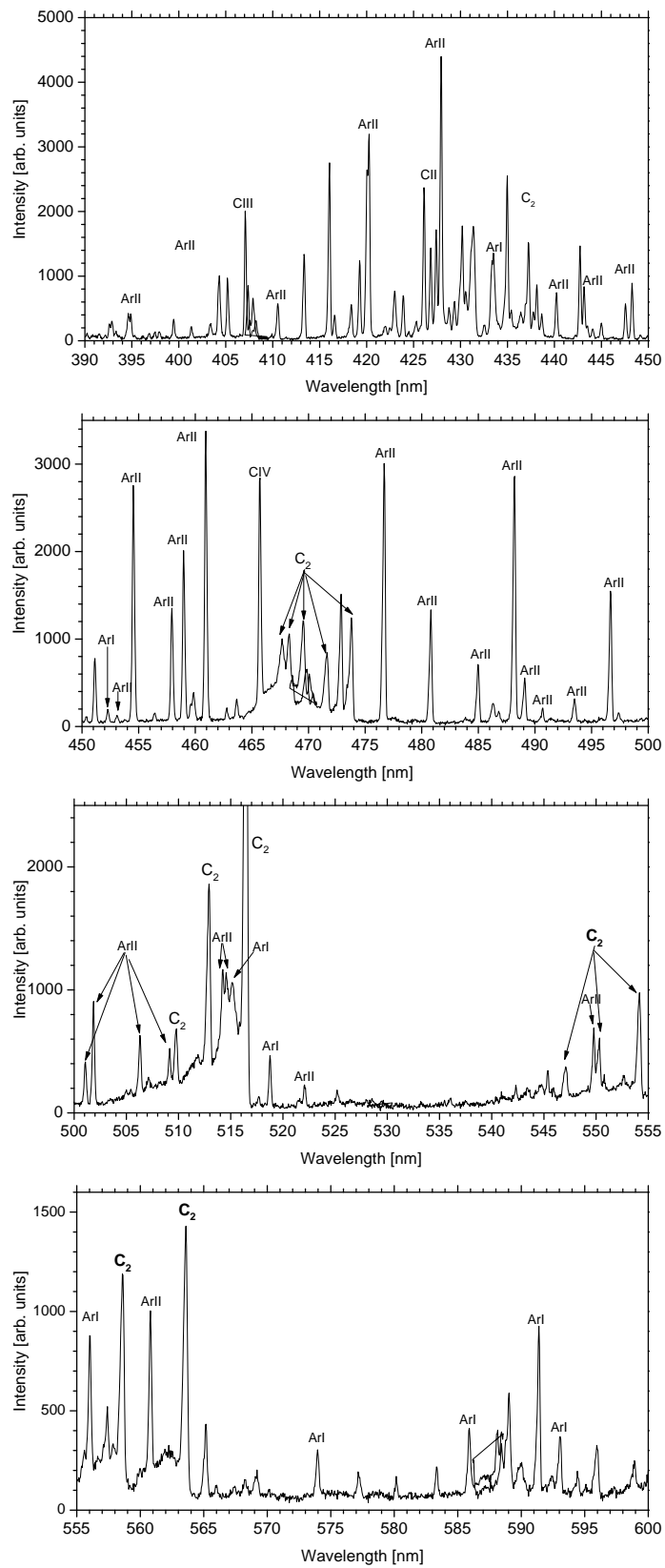


Figure 3.2: Emission spectrum from sputtering source in the wavelength range of 390–600 nm, shown in four sections.

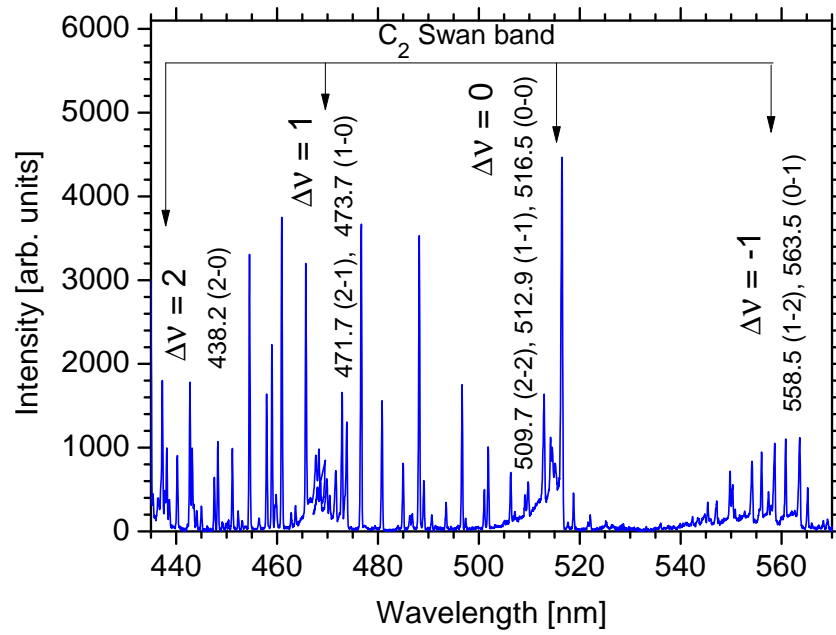


Figure 3.3: Emission spectrum of carbon glow discharge at 2.5 mbar Argon pressure, 18 mA discharge current and 200 V voltage drop across the plasma. The swan band transitions are labelled in the spectrum.

current will lead to enhanced sputtering, viz. enhanced sputter yield, and hence a greater C_2 yield.

But before making an immediate conclusion about the dominant mechanism of

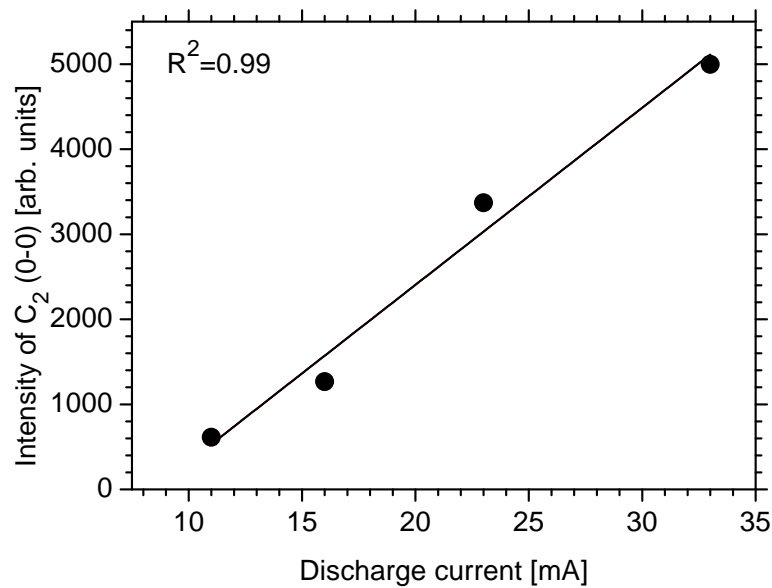


Figure 3.4: Intensity variation of Swan band head 0-0 (516.5 nm) with discharge current.

C–C association, we attempt to understand the mechanism by analyzing the pressure dependence of the vibrational temperature of C₂ and the C₂ (0–0) band head intensity. In the next section, we will see that how vibrational temperature (T_{vib}) of C₂ can be estimated using the intensities of the Swan band.

Boltzmann plot method for T_{vib} of Swan band

The Boltzmann plot method has been employed to deduct the T_{vib} of Swan band. The sums of the intensities of all bands with the same upper state or same lower state are proportional to the number of molecules in respective state. The condition for plasma to be in local thermodynamic equilibrium has been discussed elsewhere [51] and the criterion is satisfied when the electron number density exceeds a certain value. Under the thermal equilibrium condition, the population of the initial state is proportional to $\exp[-G_0(v)hc/kT]$ and the population of molecules in different vibrational levels, which follows the Boltzmann distribution [52], can be estimated using the equation 3.1.

$$\log \sum_{v'} I(v', v'') \lambda^4 = C_1 - \frac{G(v')hc}{kT_{vib}}, \quad (3.1)$$

where $I(v', v'')$ is the intensity of a transition from the vibrational level v' of the upper electronic state to the vibrational level v'' of the lower electronic state, λ is the wavelength of emission, $G(v')$ is the term value having dimensions of wave number and corresponding to the vibrational energy level v' , h is the Planck constant, c is the velocity of light, k is the Boltzmann constant, T_{vib} is the vibrational temperature and C_1 is a constant. A plot between $\log \sum I(v', v'') \lambda^4$ and $G(v')$ gives a straight line with slope $-hc/kT_{vib}$, and is known as Boltzmann plot (Figure 3.5). The vibrational temperature (T_{vib}) can be estimated using the slope.

The vibrational term value $G(v')$ [52] is calculated using the equation 3.2.

$$G(v') = \omega_e(v' + \frac{1}{2}) - \omega_e \chi_e(v' + \frac{1}{2})^2, \quad (3.2)$$

where ω_e and χ_e are the oscillation frequency and the anharmonicity of the state, respectively. The intensities of C₂ bands used for the calculation of T_{vib} are listed

Table 3.1: Intensity (arb. units) of C₂ transitions under different Argon pressure

transition (nm) (band)	1.5 mbar	2 mbar	2.5 mbar	3 mbar	3.5 mbar
473.7 (1-0)	1860	1607	1295	420	45
512.9 (1-1)	564	1174	1635	540	58
558.5 (1-2)	379	694	1052	310	0
438.2 (2-0)	1888	1434	994	322	42
471.7 (2-1)	276	520	721	222	0
509.7 (2-2)	236	436	582	198	32
516.5 (0-0)	1615	3166	4508	1454	0
563.5 (0-1)	425	828	1119	342	49

in Table 3.1 given below. The T_{vib} of C₂ is calculated by Boltzmann plot using Equations 3.1 and 3.2.

For the investigation of vibrational temperature behavior with Argon gas pressure, emission spectra are recorded under stable discharge condition with the same discharge current (18 mA) and voltage drop (200 V) conditions.

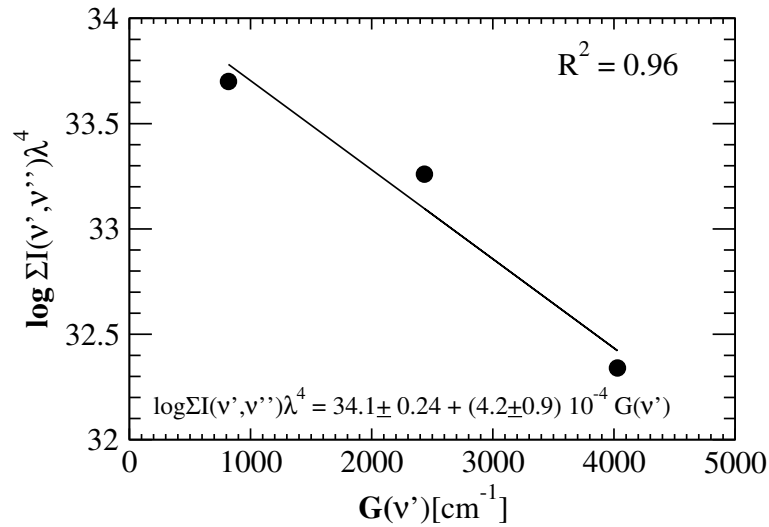


Figure 3.5: Boltzmann plot at 2.5 mbar gas pressure, 18 mA discharge current and 200 V voltage drop across the plasma. The value of $G(v')$ and $\log \Sigma I(v', v'') \lambda^4$ are estimated using equations (3.1) and (3.2). In the method of Boltzmann plot the sum of intensities of all bands with the same lower state are considered and therefore eight transitions provide three points for linear fit.

Effect of Argon pressure on C_2 (0–0) band intensity and T_{vib}

The energy for excitation comes almost entirely from collision with Argon ions. For a fixed discharge current and discharge voltage, the energy available for vibrational excitation is therefore a function of pressure alone. Our results indicate that C_2 formation and its vibrational temperature are strongly affected by the Argon gas pressure. The C_2 (0–0) intensity goes through a maximum in the same pressure range (at an ambient pressure around 2.5 mbar), when the discharge current is kept fixed (Figure 3.6). It should be noted, that we are using the 0–0 band head intensity as a proxy for C_2 formation, but this proxy is no indicator of the existence of C_2 in higher excited states.

Over the same range of ambient pressures T_{vib} shows a decreasing trend (Figure 3.6). This suggests that the range of pressures considered is optimum for C_2 formation in low vibrational states by three-body collision. If the pressure is lower, not only does three body association, but also collisional quenching of the vibrationally excited states becomes less likely and the fraction of the population in high vibrational states is relatively larger. This explains the inverse trend of T_{vib} with

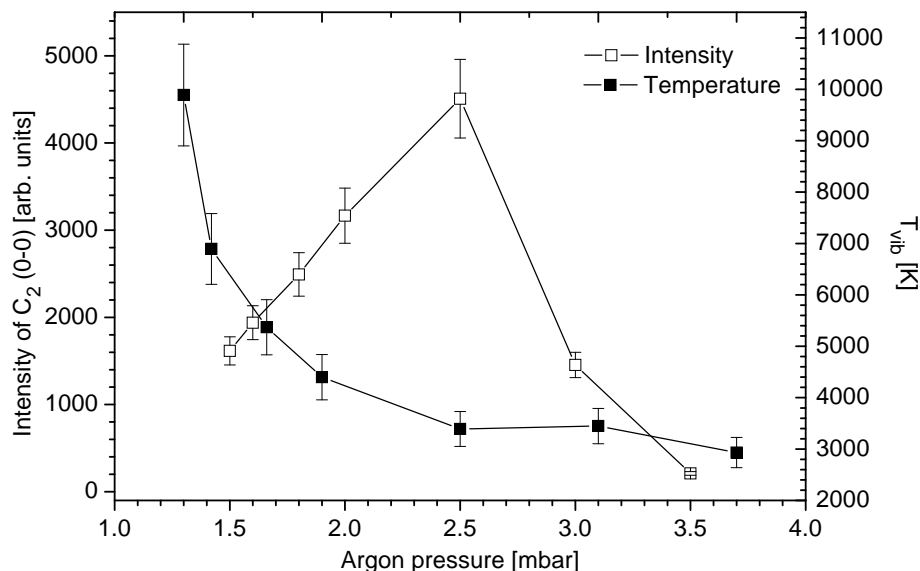


Figure 3.6: Variation of intensity of C_2 band head and the associated vibrational temperature of C_2 as a function of the ambient pressure. Lines joining the symbols are an aid to eye. The error bars represent the experimental error in both the intensity and the vibrational temperature. The variation of the two parameters shows that the optimum pressure for clustering is 2.5 mbar.

pressure.

We have repeated our experiment with N₂ ambient, instead of Argon, and in that experiment we observed intense emission corresponding to the C–N (0–0) band, but not the C–C (0–0) band. Under identical conditions of discharge current and ambient pressure, the C–N emission (under nitrogen ambient) is at least an order of magnitude higher than the C₂ Swan band (under Argon ambient). The appearance of the CN band can be understood as arising from a C–N₂ three-body association, while the suppression of C–C association in N₂ ambient could be because the three-body association preferentially leads to C–N association at the expense of C–C association. This gives credence to the inference, that three-body association is the dominant mode of clustering in the present set-up.

3.3 OES investigation of laser ablation source

The interaction of high intensity laser pulse (10^9 Wcm^{-2}) with solid surface lead to the formation of plasma plume. The ejecta in the plume are hot species and in order to form clusters, they need to be cooled down. High pressure gas pulses may serve this purpose. The laser pulse and gas pulse should be synchronized such that there must be an overlap between the plume and gas pulse. The collisions between the gas atoms and carbon ejecta may lead to the production of clusters.

The primary process in cluster formation is the production of a dimer by three body collision. The yield of clusters heavier than dimer strongly depends upon the yield of a dimer. In this section, formation of carbon clusters resulting from the interaction of ablated carbon atoms with ambient Argon atoms is discussed. The effect of the type of gas, delay and gas pulse duration on cluster formation are also points of discussion.

Significance of delay on cluster formation

The key factor for cluster formation is found to be the delay between laser pulse and gas pulse. It has a very strong influence on the C₂ yield. The synchronization between the gas pulse and the laser pulse is vital for the cluster formation. The

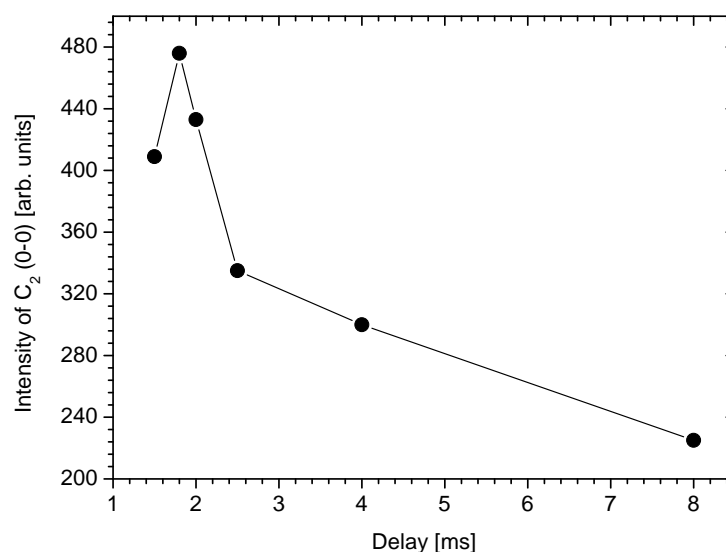


Figure 3.7: Intensity variation of Swan band head 0–0 (516.5 nm) with the delay between gas pulse and laser pulse.

synchronization need to be such that plasma plume should be produced when the peak of the gas pulse passes the target surface. We have systematically changed the delay for maximum C₂ yield. The optimized delay for maximum C₂ yield is found to be 1.8 ms in the present source. The variation of C₂ (0–0) Swan band head with the delay is shown in Figure 3.7.

Formation of C₂(0–0) Swan band

The analyzed emission spectra from laser ablation of graphite disk in the presence of high pressure Argon gas pulse reveal the formation of neutral C (193 nm) and C₂ Swan band. An emission spectrum is shown in Figure (3.8). C₂ is formed by three body collision between the ambient Argon atoms and carbon ejecta. It was confirmed that in absence of the ambient gas, C₂ Swan band does not form in the emission spectrum.

Dependence of C₂ yield on type of gas and gas pulse duration

It has been observed that cooling of the energetic ejecta is influenced by the type of gas. In addition to that, gas pulse duration is also found to be a crucial parameter

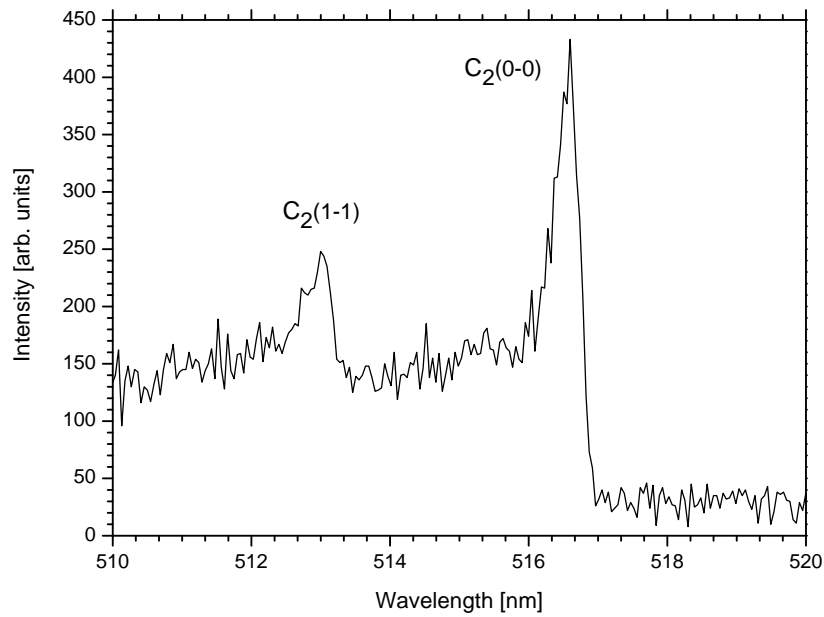


Figure 3.8: Emission spectrum of C₂ Swan band in the presence of Argon gas.

for cooling phenomena of ejecta.

The ejecta in the plasma plume are hot enough and in order to form C₂, cooling of atomic ejecta is essential. We have verified the importance of the type of ambient gas (atomic or molecular) required for the cooling. For this purpose, Argon gas and

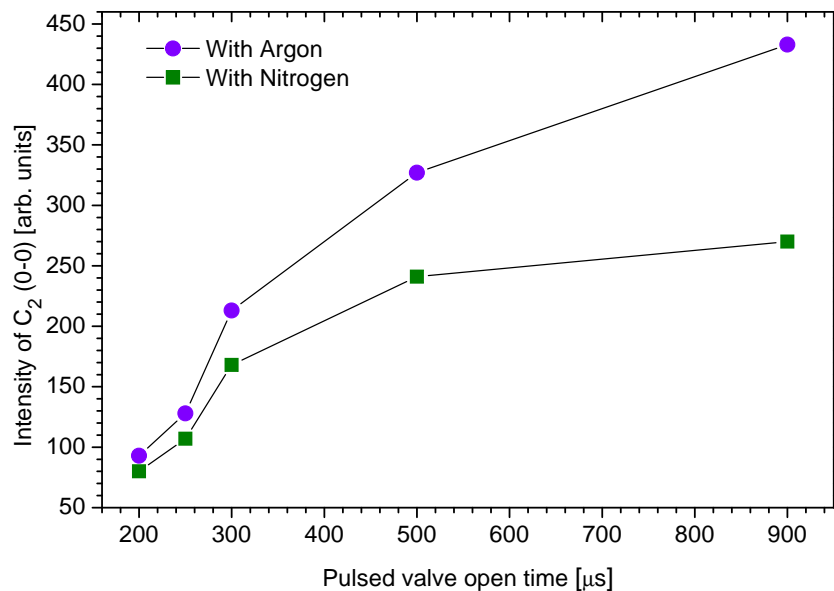


Figure 3.9: Intensity variation of Swan band head 0-0 (516.5 nm) with pulsed gas ON time in presence of two different gas (Argon and N₂).

N_2 gas have been used to cool down the atomic ejecta in plume. It is observed that cooling is more prominent under Argon gas environment than N_2 gas (Figure 3.9). It has also been found that the intensity of C_2 increases with the gas pulse duration (ON time), as the number density of ambient gas also increases (Figure 3.9).

As a concluding remark of this chapter, control over the formation of C_2 in hollow cathode sputtering source and laser ablation source would be helpful for performing the mass spectrometric study of carbon clusters. The mass spectrometric analysis from these sources are discussed in the chapter 4.

Chapter 4

Mass spectrometric study of clusters

4.1 Time-of-Flight (TOF) Mass Spectrometry

Optical emission spectroscopy has been used to detect carbon clusters in the sooting environment. But emission spectroscopy has its own limitation as not more than carbon dimer can be detected due to the unavailability of spectroscopic information. Thus for detecting large mass clusters, time-of-flight (TOF) mass spectrometric technique is our choice because it is suitable for a continuous beam source (sputtering source) as well as for a pulsed source (laser ablation and pulsed nozzle). In time-of-flight mass spectrometer (TOFMS), there is no upper mass limit provided a suitable ionization method is used, a complete mass spectrum can be recorded with very fast speed (within μs), and its efficiency depends on the electronic settings rather than depending on the mechanical alignment and formation of uniform and stable magnetic fields.

Working principle

The most common TOFMS configuration is Wiley-McLaren [53] type. The schematic diagram of a two field Wiley-McLaren TOFMS is shown in Figure 4.1. Ions are produced in the first region, this region is called the interaction region. Ions are pushed in to the second region by applied electric field (E_s). The second region is called acceleration region, ions are pushed by the applied field (E_d) into

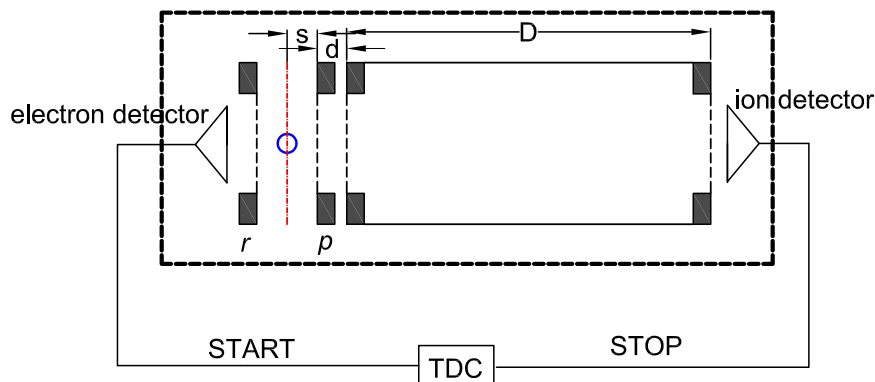


Figure 4.1: Schematic diagram of TOF mass spectrometer. The blue circle represents the ionization volume, red dashed line represents the plane for incoming ionizing beam and target beam. First plate (r) is used to repel ions and second plate (p) is used to push the ions towards the detector. The plates have high transmission meshes.

a region which is field free and is known as the drift region. Ions are separated in the field free region according to their mass to charge ratio. Thus TOFMS is used for separating ions according to their mass to charge ratio by measuring their flight time.

Ions are produced either by a continuous ionizing source or by a pulsed ionizing source. The flight time measurement of ions is either triggered by the detection of electron, produced due to ionization, or by the pulse from the ionizing source (such time reference is derived from electron pulse or laser pulse) and is stopped by the ion detection. When the flight time measurement is carried out using electron as start and ion as stop, the TOFMS is said to be operated in electron-ion coincidence mode and when the flight time measurement is triggered by the ionizing pulse then the TOFMS is said to be operated in pulsed mode.

Detectors

For the detection of ions and electrons, microchannel plate (MCP) and channeltron electron multiplier (CEM) detectors are generally used. Both the detectors work on the principle of electron multiplication. The schematic diagrams of a two stage MCP (known as Chevron MCP) is shown in Figure 4.2. A MCP is made from highly resistive material and is an array of millions of miniature electron multipliers oriented parallel to one another [54]. Each channel can be considered as a separate

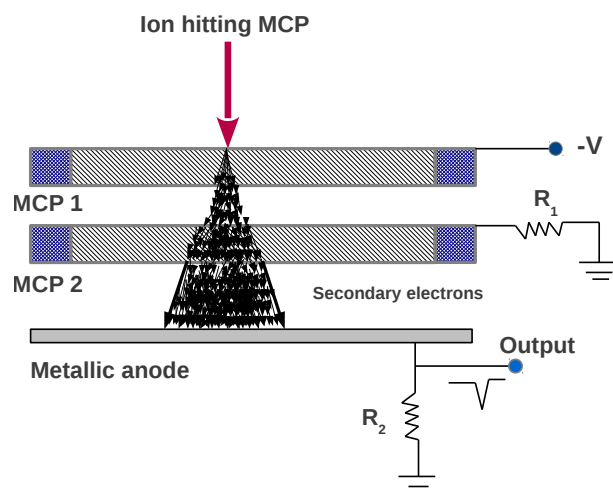


Figure 4.2: Schematic diagram of Chevron microchannel plate detector and pulse derivation circuit for cations, $R_1 > R_2$.

electron multiplier. When a charged particle or photon hits the front surface of MCP, it enters into the channel. The impact of particle with the wall of channel is most probable as channels are at an angle with respect to the plate. Particles hitting the wall of channel generate electrons from its surface. These electrons strike with the wall of channel and generate secondary electrons. This process lead to the electron multiplication and finally bunch of electrons are released from the output end.

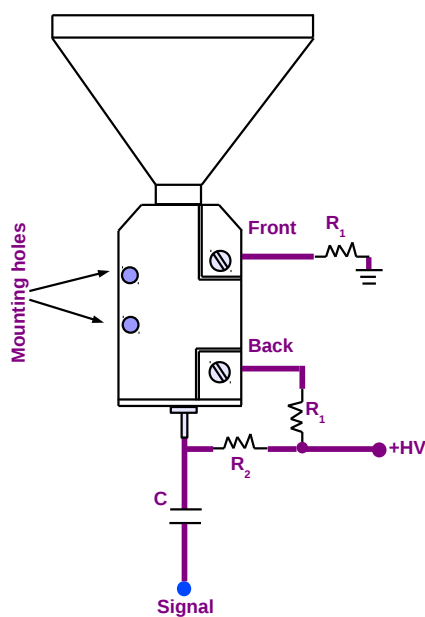


Figure 4.3: Schematic diagram of channel electron multiplier detector and pulse derivation circuit for anions, $R_1 > R_2$.

Similarly, CEM also works on the principle of secondary electron emission. The schematic diagrams of CEM is shown in Figure 4.3. The funnel shaped aperture of CEM is made from highly resistive material. When a charged particle or photon impinges on its funnel shaped active area, secondary electrons are produced. These electrons get accelerated by the bias voltage, strike the wall and produce further electrons. The gain of Chevron MCP and CEM is in the range of 10^7 . The mass and energy of an ion affect the detection efficiency of MCP detector. The detection efficiency correction is essential and will be discussed in this chapter.

Ion trajectory simulation

By following the Wiley-McLaren criteria [53], electric fields in the different regions of TOFMS can be estimated provided the lengths of spectrometer are fixed. To demonstrate the trajectory of ions of a particular mass under the influence of electric fields, an ion trajectory simulation is carried out. The ion trajectory simulation is performed using SIMION 8.0 package. The influence of electric fields on the ion trajectories is verified.

Simulation of ion trajectories shows that Xenon cluster ions up to size 50 are transmitted without loss under the present experimental conditions (see table 4.1). Cluster ions heavier than Xenon cluster ion of size 50 are expected to be detected by MCP only if their velocity vectors point slightly away from the expansion direction prior to ionization.

TOF experimental setup

Two separate TOF spectrometers are used for the detection of cluster ions. First TOFMS with shorter drift tube (15 cm) has been used for the detection of cluster ions from the sputtering source on the basis of electron-ion coincidence mode. The resolving power of TOF spectrometer in the electron-ion coincidence mode is 120. Ions are detected by a 40 mm diameter Chevron MCP detector (*Photonis*) and the time measurement is carried out using a Time-to-digital converter (TDC). Electrons produced in the ionization of clusters are detected by a 25 mm diameter Channel

Table 4.1: Specifications of TOF mass spectrometers

s (cm)	d (cm)	D (cm)	E_s (V/cm)	E_d (V/cm)	Resolving power	TOF mode used	Cluster source
0.6	0.6	15	333	1533	120	coincidence	Sputtering
1.2	0.8	50	250	2500	340	pulsed mode	Nozzle

electron multiplier (CEM) detector (*Sjuts*).

To resolve a heavy mass cluster ion (A_n) from a mixed cluster ion (A_nB), containing parent cluster ion and a molecule, high mass resolution spectrometer is required. For this purpose, another TOFMS with longer drift tube (50 cm) and improved mass resolution has been employed. The resolving power of this TOFMS in the electron–ion coincidence mode is 340, which may be taken as the intrinsic resolving power of the spectrometer. In addition to that, second TOFMS is equipped with two deflectors and a lens for steering and focusing the heavy cluster ions towards the ion detector. Ions are detected by a 40 mm diameter Chevron MCP detector (*Photonis*). The time measurement is carried out using a multi-hit flash TDC, which is able to accept a peak ion count rate of 1 GHz and have the sweeping time upto 68.7 s, suitable to detect heavy cluster ions. The specifications of both spectrometers are provided in table 4.1.

TOFMS is pumped by a combination of turbo pump (520 l s^{-1}) and a scroll pump is employed to create vacuum in chamber housing the TOFMS. The minimum pressure achieved in first TOFMS chamber is 5.5×10^{-8} mbar and in second TOFMS is 2×10^{-7} mbar.

Ionization scheme for clusters

Continuous UV source

Sputtering source generate clusters in a continuous beam form. Clusters from sputtering source are ionized using a continuous He-microwave discharge UV source. The microwave discharge lamp is a very compact light source. It is an electrode less discharge lamp and this makes it contamination free ionizing source.

He-gas is used as a discharge gas with 2.45 GHz microwave up to microwave power of 50 W. The discharge is established in a quartz tube (8 mm o.d. and 4 mm i.d.) intersecting a microwave cavity. A needle valve is used to control the He gas flow inside the quartz tube. The discharge is initially triggered by a Tesla coil. In the present case, radiation of 21.21 eV energy is produced using He as a discharge gas. For preventing the heating and breaking of quartz tube, tube is cooled by flowing air around the discharge region.

Pulsed Nd:YAG laser

Laser ablation source and pulsed nozzle source generate clusters in pulsed form. Ionization of these clusters by a continuous ionizing source will lead to an enhanced false ion count in the mass spectrum due to the low duty cycle of cluster beam. In this case, clusters from a pulsed cluster source are ionized using a pulsed ionizing source, Nd:YAG laser. An Nd:YAG (*Continuum*) laser is employed to ionize the supersonic gas pulses from the pulsed nozzle in the ionization region of TOFMS. Frequency tripled output of the Nd:YAG laser at 355 nm having a fluence of 61 Jcm^{-2} has been used in most cases. Pulse width of 8 ns and repetition rate of 30 Hz is fixed for all measurements. In order to attain efficient ionization of clusters, gas pulse is synchronized with the laser pulse. The correct timing is essential between these two pulses are important for the cluster ion production.

Laser pulse is used as a master trigger for the flight time measurement of cluster ions. The synchronization between the laser pulse and the gas pulse, for pulsed nozzle source, is shown in Figure 4.4.

Calibration of TOFMS

To get a calibration equation for TOFMS, first it is operated with known gas. Second, the mass resolution of TOFMS is optimized by changing the experimental parameters, such as, spectrometer voltages, overlap of effusive beam and ionizing source beam, minimization of the ionization volume. Once the resolution of spectrometer is optimized for these experimental parameters, these entities are kept fixed

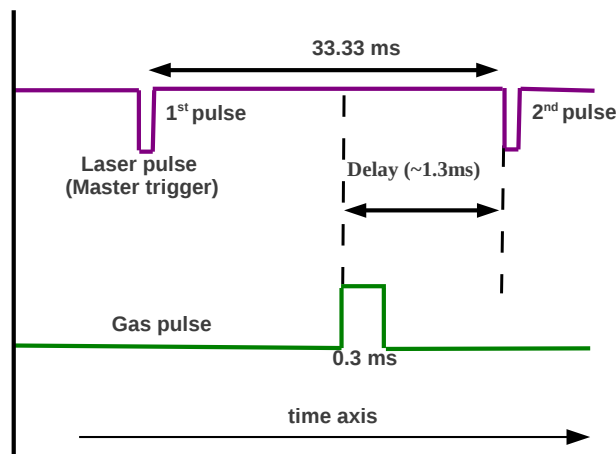


Figure 4.4: Schematic diagram of gas pulse and laser pulse synchronization, for cluster ion production, using pulsed nozzle source and Nd:YAG laser, Figure not to scale.

for the unknown gas sample. To get a precise calibration equation for TOFMS, it is better to have many known ions over a wide mass range in the mass spectrum. For this purpose, generally, a gas with many isotopes (Krypton or Xenon) is used.

The TOFMS is calibrated for Krypton ions produced by ionizing an effusive

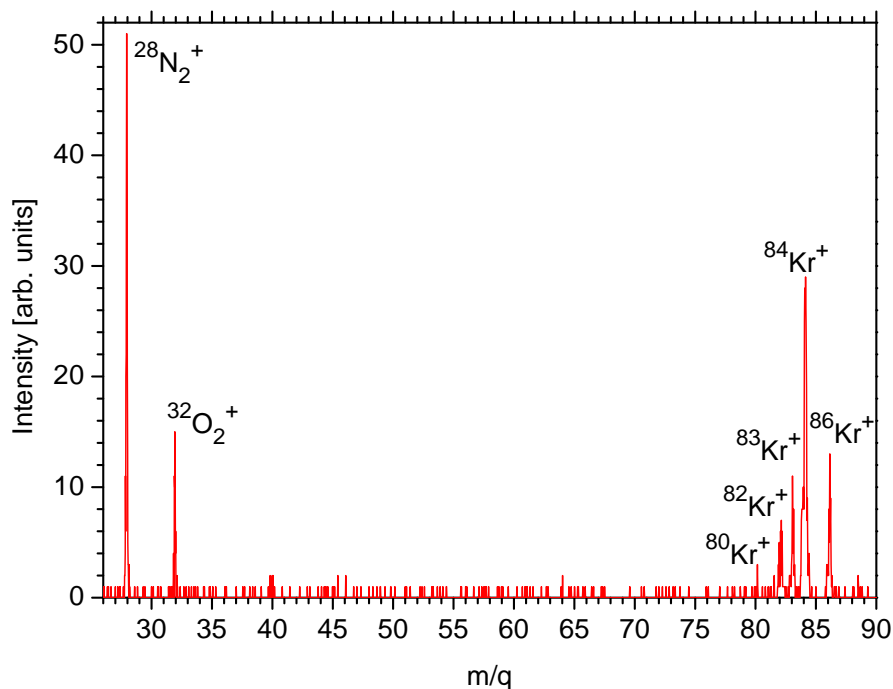


Figure 4.5: A mass spectrum obtained from the ionization of Krypton effusive gas jet by He-discharge UV source. The resolving power of spectrometer is 340.

Krypton beam using a He-discharge UV source. A mass spectrum of Krypton ions has been shown in Figure 4.5. Nitrogen and Oxygen ions are also present in the mass spectrum due to the impurity in Krypton gas.

The flight time distribution of an ion have finite broadening due to the initial momentum of ions and spread in the ionization volume. Ions with zero momentum and flight time (T) appears at the center of the TOF profile. Once the flight time (T) and mass to charge ratio of each ions is known, graph can be plotted between the flight time (T) of ions and $\sqrt{\frac{m}{q}}$ to get a calibration equation for unknown masses. The calibration equation of TOFMS is of the form,

$$T = \sqrt{\frac{m}{q}}A + B \quad (4.1)$$

here A and B are constant and can be estimated by linear fitting (Figure 4.6) between T and $\sqrt{\frac{m}{q}}$.

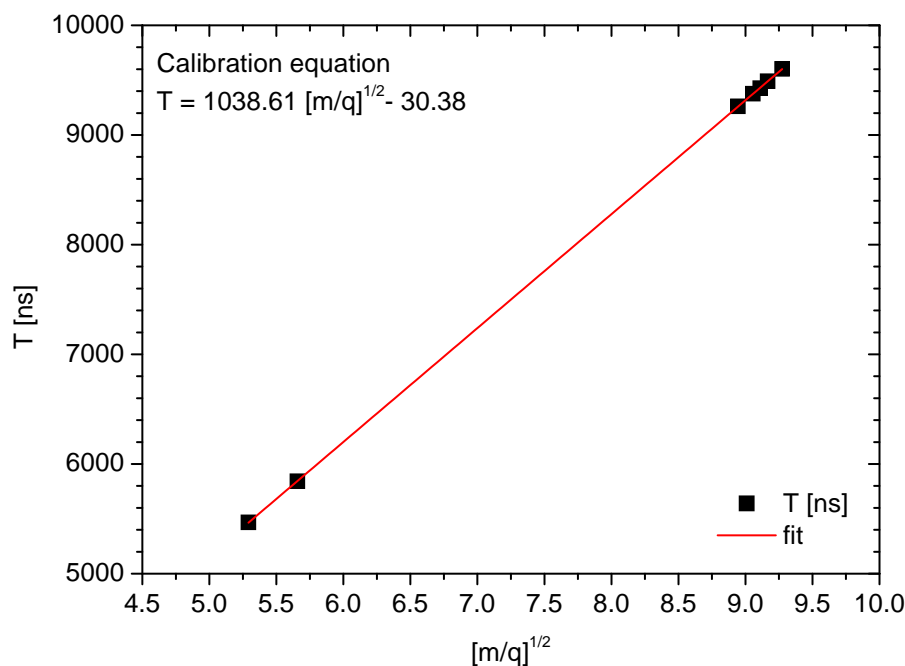


Figure 4.6: A graph between the flight time (T) and square root value of mass to charge ratio of ions for finding the calibration equation.

Once the calibration equation has been obtained, this equation can be used for identifying the unknown masses provided that electric fields and the mechanical alignments of spectrometer have not been disturbed. If it is the case, the calibration

exercise has to be performed each time before doing the experiment.

4.2 Graphite sputtering source

The formation of carbon dimer in the sooting environment of hollow cathode sputtering source has been studied using emission spectroscopy and was discussed in previous Chapter . For the detection of heavy clusters, TOF mass spectrometer is used. The sputtering source is used to generate a beam of carbon clusters. Argon gas is used as a discharge gas as well as carrier gas for carbon clusters in the sputtering source. The gas jet carry clusters from the cavity of source to the ionization region of TOFMS. Clusters are ionized by He-discharge UV source. Flight time measurement of cluster ions is carried out in electron-ion coincidence mode.

Carbon clusters and mixed clusters of carbon and Argon

In the present source, Argon gas jet is capable to transport carbon clusters upto a distance of 40 cm where the center of interaction region of TOFMS is situated. During the transport of clusters to TOFMS, three body collision between the carbon

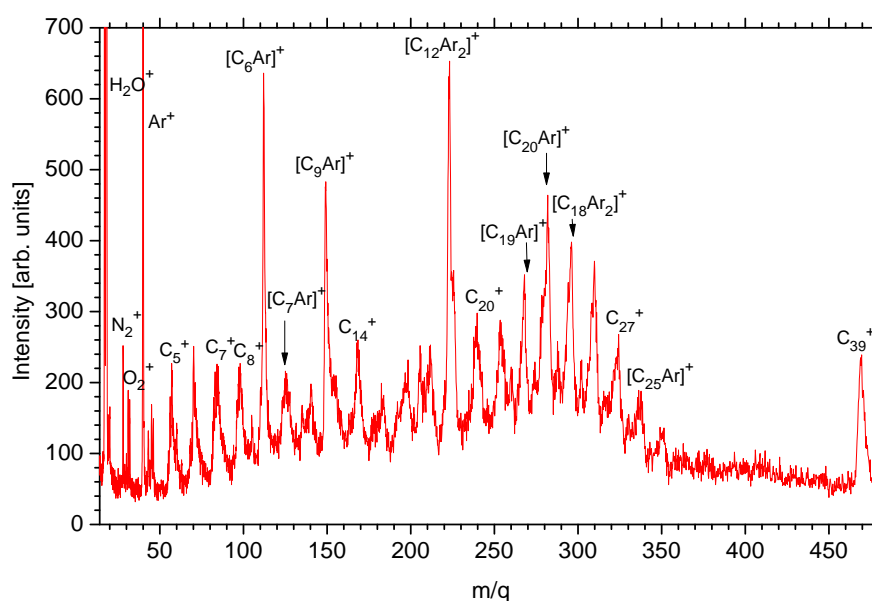


Figure 4.7: Mass spectrum of carbon cluster ions and mixed cluster ions of carbon and Argon obtained by ionizing clusters from sputtering source using He-discharge UV.

clusters and Argon atoms may also lead to the adsorption of Argon atoms on the surface of clusters. A mass spectrum of cluster ions is shown in Figure 4.7.

The spectrum is acquired when the voltage drop across the plasma and discharge current are 300 V and 17 mA respectively, an Argon pressure of 1.7 mbar is maintained for stable plasma formation. In addition to the formation of carbon clusters, mixed clusters of carbon and Argon are also observed.

4.3 Clusters from pulsed nozzle source

Pulsed nozzle source has been used for generating clusters from gas species. High pressure gas pulses are ejected by a pulsed nozzle (1 mm diameter), these pulses are extracted through a conical skimmer (1.2 mm diameter) placed at 20 mm from the nozzle. For a mass spectrometric analysis of the clusters, it is necessary to have a pulsed ionization source. This is achieved by the use of 355 nm Nd:YAG laser pulses downstream the expansion at a distance of 17 cm in the ionization gap of the TOFMS described earlier. Before going to the results of this study, we look at the ionization mechanism under intense laser pulses.

Multi-photon ionization (MPI)

The discovery of high intensity pulsed laser laid the foundation of an ionization scheme in which an atom may get ionized by the absorption of photons even when the photon energy is less than the ionization energy of atom. This ionization scheme is popularly known as multiphoton ionization (MPI). The interaction of an atom with high intensity laser pulse (10^7 - 10^{15} Wcm⁻²) may lead to the simultaneous absorption of more than one photons by the virtual states of atom. The life time of these states is very short and is of the order of one optical pulse. When the energy of the photons absorbed by an atom overcome the ionization barrier, atom gets ionized and this process is known as multiphoton ionization (MPI). The multiphoton ionization process was first observed by Voronov et al. in the ionization of Xenon atoms via seven photon absorption [55]. The laser parameters, such as, intensity, pulse width and wavelength play a significant role in MPI. Optical energy absorption is

more prominent in clusters than their constituent atom or bulk.

The intensity (I) of a laser pulse can be calculated using equation 4.2.

$$I = \frac{\epsilon_0 c E^2}{2} \quad (4.2)$$

where c is the speed of light, ϵ_0 is the permittivity of space and E is the magnitude of electric field. When an atom interacts with laser pulse, the influence of laser field strength on the electron cloud in atom is more prominent when the laser intensity approaches or exceeds the nuclear electric field experienced by the electron in the first Bohr orbit of atomic hydrogen. In this case, bound electrons in the outermost orbit of atom overcome the ionization barrier and this type of ionization is known as field ionization. The Coulomb field (E_a) experienced by an electron in the first Bohr orbit of atomic hydrogen is given in equation 4.3.

$$E_a = \frac{e}{4\pi\epsilon_0 a_0^2} = 5.1 \times 10^9 \text{ V cm}^{-1} \quad (4.3)$$

The field strength of laser at intensity $3.5 \times 10^{16} \text{ W cm}^{-2}$ corresponds to the Coulomb field (E_a) experienced by an electron in the first Bohr orbit of atomic hydrogen. The probability per unit time (P) of ionizing an atom or ionization rate [56] depends on the intensity (I) of laser and number of photons (N) per pulse and is given in equation 4.4,

$$P = \sigma_N I^N \quad (4.4)$$

The number of photons in a coherence volume (λ^3) can be estimated using equation 4.5,

$$N = \frac{I\lambda^3}{c\hbar\omega} \quad (4.5)$$

where I is the intensity of laser, $\hbar\omega$ is the energy of photon and λ is the wavelength of laser.

The ionization mechanism can be further separated into two different ionization regime, MPI and tunneling ionization, on the basis of Keldysh parameter (γ) [57].

The Keldysh parameter (γ) is defined as,

$$\gamma = \sqrt{\frac{I_p}{2U_p}} \quad (4.6)$$

where I_p is the ionisation potential of atom in eV and U_p is the pondermotive energy of the quivering electron in the laser field [57]. The pondermotive energy or the quivering energy of the quasi-free electron in a laser field is given as,

$$U_p = \frac{e^2 E^2}{4m\omega^2} = 9.33 \times 10^{-14} \times I \times \lambda^2 \text{ eV} \quad (4.7)$$

where E is the laser field strength, ω is the photon angular frequency, I is the intensity in W/cm^2 of the optical pulse and λ is the wavelength in μm [58].

If $\gamma > 1$, the ionization is via non-resonant multiphoton ionization followed by the simultaneous absorption of many photons [8–10, 59].

$$A + N\hbar\omega = A^+ + e^-$$

In this interaction, the energy of $N\hbar\omega$ is greater than the ionization potential (I_p) of atom. For $\gamma < 1$, the ionization is explained by tunnel ionization [58] and is not the case in present study.

Atomic clusters: Xenon

The first target chosen for the study was Xenon clusters. Since the setup consist of a pulsed gas and a pulsed laser, correct timing synchronization between the two pulses is very important to achieve a cluster ion mass spectrum. The timing between two pulses may change according to the mass and ratio of specific heat of the gas used. To check the influence of delay (see Figure 4.4) between laser pulse and gas pulse on the mass spectra, delay has been varied between 1.0–1.6 ms in the present experiment, based on the delay range estimated from calculations. By changing the delay in step of 0.1 ms, laser pulse may collide with any portion of the gas pulse as the gas pulse remains open for 0.3 ms (Figure 4.8). It is found that changing

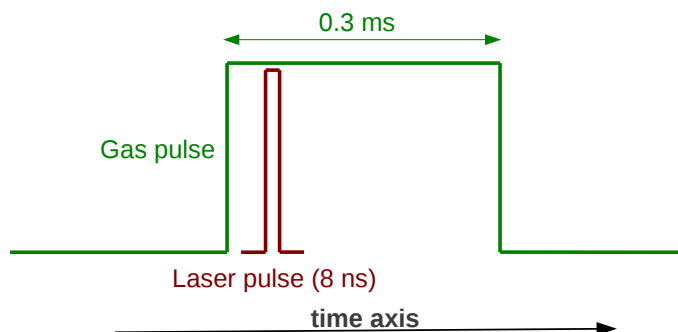


Figure 4.8: A schematic diagram of interaction of Nd:YAG laser pulse with the gas pulse ejected by a pulsed nozzle. Pulsed nozzle and laser operation was set at 30 Hz. The delay between laser and gas pulse is changed in step of 0.1 ms to observe the variation in cluster ion production, Figure not to scale.

the delay within time window of gas pulse duration 0.3 ms results in change in intensities of cluster ions. This shows that clusters distribution is non uniform in the gas pulse.

Mass spectra of Xenon cluster ions with different delays are recorded and are shown in Figure 4.9. It is clearly seen (Figure 4.9) that cluster ion production remains within the Xenon gas pulse which is open for 0.3 ms.

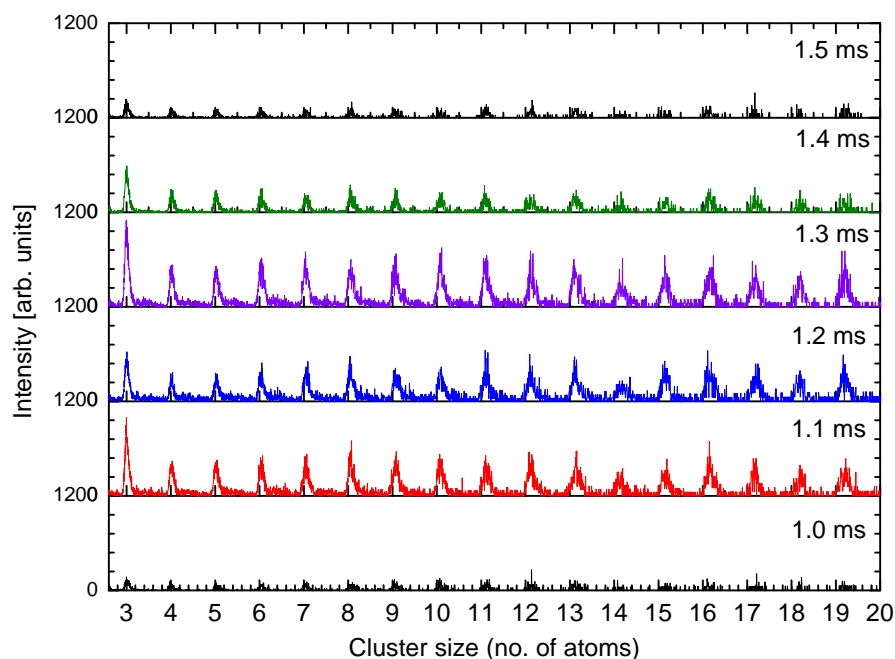


Figure 4.9: Effect of the delay between gas pulse and laser pulse on the cluster ions.

Correction in detection efficiency for heavy masses

The mass, composition and energy of an ion affect the detection efficiency of MCP detector. A correction factor for the detection efficiency of ions is needed. The efficiency falls rapidly as the mass increases and ion energy decreases [60]. The curve described by Gilmore et al. has been used for finding the detection efficiency of MCP for Xe cluster ions at ion energy of 2 keV.

An equation for the correction factor is obtained by fitting (Figure 4.10).

$$efficiency = \frac{43.01}{m + 14.27} \quad (4.8)$$

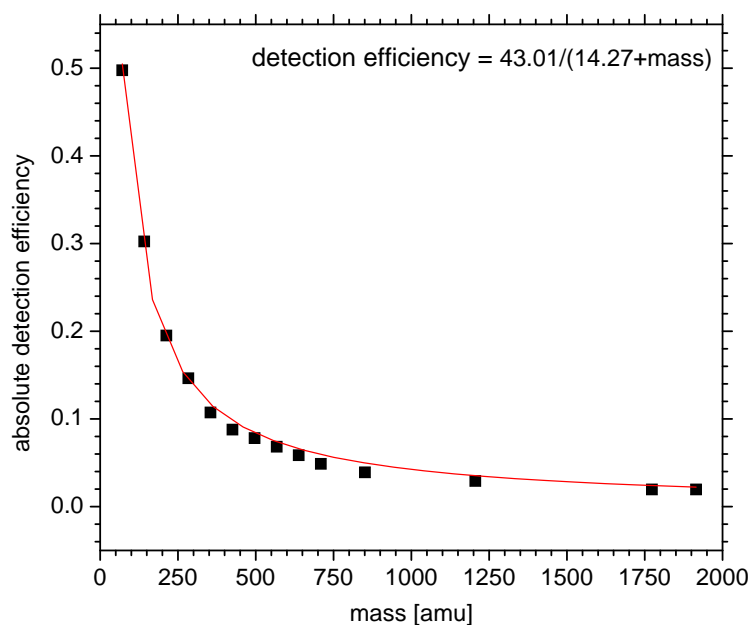


Figure 4.10: A graph showing the fitting between the detection efficiency and mass of cluster ions. These parameters are estimated from the study by Gilmore et al. [60].

The equation 4.8 has been used for intensity correction in the Xenon cluster ions. To perceive the effect of the efficiency correction in the intensity of Xenon cluster ions, two mass spectrum with and without the efficiency correction have been shown in Figure 4.11. Xenon cluster ions up to size 70 are seen in the mass spectrum. A significant difference in the intensity of cluster ions has been observed after inserting the correction factor in the mass spectrum.

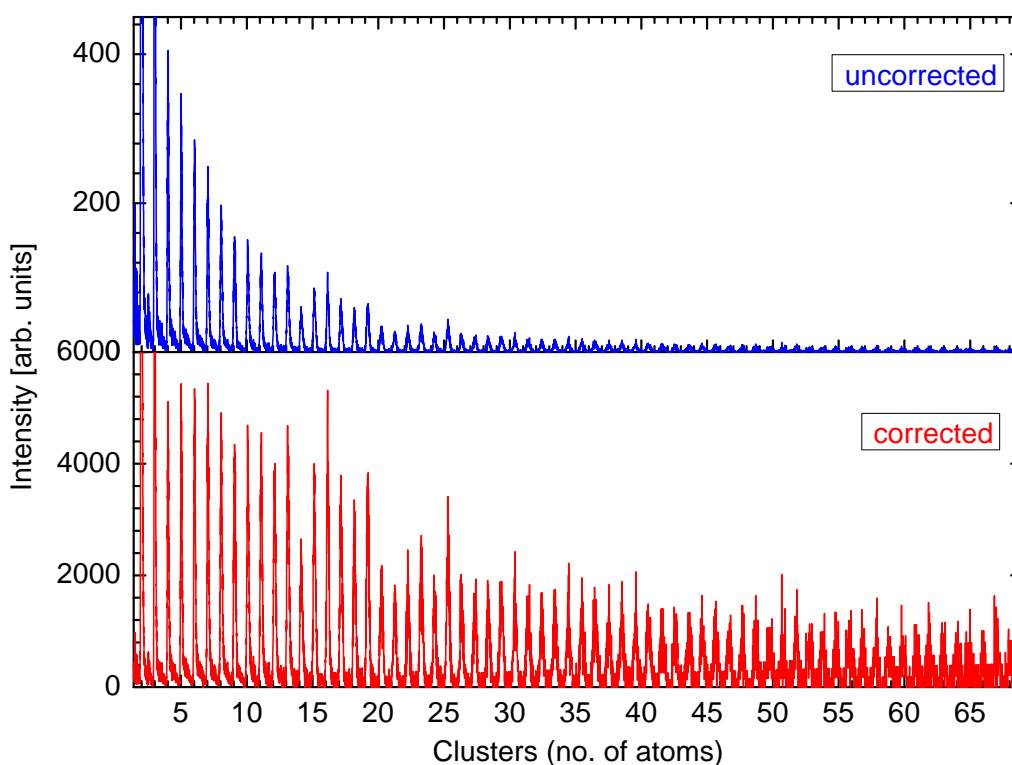


Figure 4.11: Xenon cluster ion mass spectrum. Upper spectrum is without correction and lower spectrum is after the correction.

Effect of stagnation pressure

The cluster ions mass spectra at different stagnation pressure condition can deliver the information for mean cluster ion size. By treating mean cluster ion size as a proxy for neutral cluster size, the influence of cluster size on multiply charged ions can be investigated.

The effect of stagnation pressure on the cluster ion yield is shown in Figure 4.12. It is found that heavy clusters are formed at higher stagnation pressure, this observation is consistent with the Hagen's theory discussed in chapter 2. A study of the dependence of the mass spectrum on the stagnation pressure, is indirectly an investigation of the dependence of cluster ion formation on the neutral cluster size. Ionization with intense UV irradiation is a simple multi-photon process, which depends on the ionization potential and not on the size of the ionized entity, as long as the size is not comparable to the UV wavelength. The size condition is satisfied as can be verified by a theoretical estimate of the mean neutral cluster size based

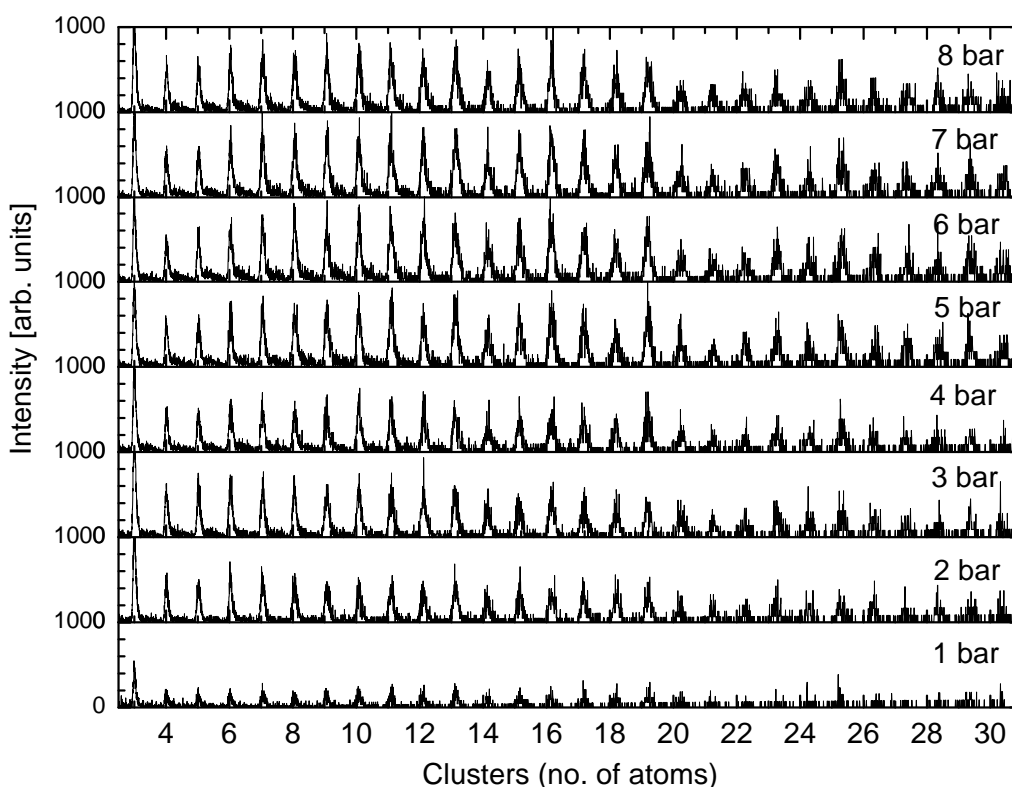


Figure 4.12: Effect of the stagnation pressure on the cluster ions.

on the Hagena theory [13] and Wigner-Seitz packing geometry [42].

Under 355 nm irradiation, the mean cluster ion size, $\langle n \rangle$, is estimated on the basis of the yield of cluster ions and their size (no. of atoms in a cluster) using equation (4.9).

$$\langle n \rangle = \frac{\sum_2^{30} (n_i N_i)}{\sum_2^{30} (N_i)} \quad (4.9)$$

The variation of the mean cluster ion size with stagnation pressure is shown in Figure 4.13. The mean cluster ion size of Xenon clusters increases with the stagnation pressure, as does the neutral cluster size according to Hagena's theory.

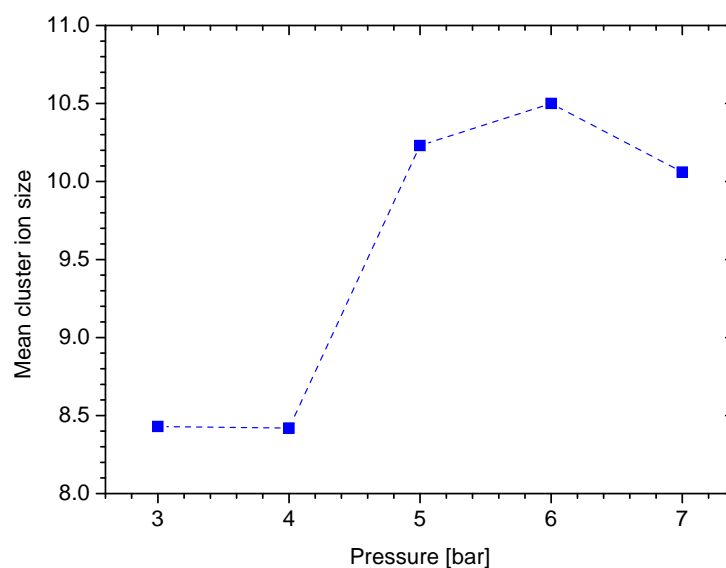


Figure 4.13: Variation of cluster ion size with the stagnation pressure under 355 nm irradiation. Lines are guides to the eye.

4.4 Molecular and mixed clusters from pulsed nozzle

Molecular clusters: Ethyl alcohol

Besides generating the atomic clusters, molecular clusters are also produced using the pulsed nozzle source. For generating molecular clusters, sample is vaporized in the high pressure pulsed driver gas. The sample is attached in the inlet gas line and is heated to create the vapor. The carrier gas can be any inert gas, in our case it is Xenon gas. The high pressure (2-4 bar) carrier gas is used to generate the clusters from the vapor by three body collision between the sample vapor atoms and Xenon atoms. During the collision, carrier gas atoms extract the excess heat away from the vapor atoms leading to the cluster formation. Using this method, Ethyl alcohol clusters $(C_2H_5OH)_n$ upto size 10 are produced. The boiling point of Ethyl alcohol is 352 K. Ionization is carried out at 355 nm laser pulse. The mass spectrum, obtained in the same experimental conditions, one with carrier gas only and another in the presence of Ethyl alcohol vapor are shown in Figure 4.14.

The bottom mass spectrum is recorded when Xenon gas expands freely through a pulsed nozzle. In this case, Xenon cluster ions are seen in the mass spectrum. In the top spectrum, alcohol is heated to produce the vapor, and this vapor is mixed

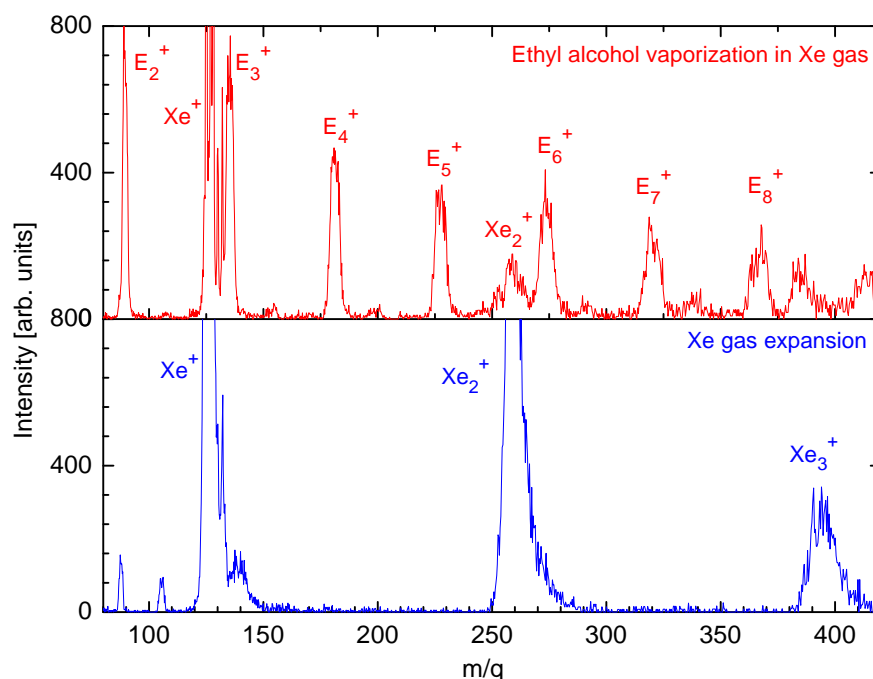


Figure 4.14: Bottom panel; Xenon gas expansion through a pulsed nozzle, leads to the formation of Xenon clusters. Top panel; Ethyl alcohol vapor is introduced in the Xenon driver gas, leads to the production of Ethyl alcohol clusters and Xenon clusters.

in the Xenon carrier gas. In this case, Ethyl alcohol cluster ions as well as Xenon cluster ions are formed in the mass spectrum.

Mixed clusters: Water vapor, Ethyl alcohol and Benzene

The pulsed nozzle has been used to generate atomic as well as molecular clusters. Although, Xenon clusters are easily formed and detected, it results in complicated distribution of cluster masses, due to the large number of Xenon isotopes. If another molecule gets attached to such clusters, it will be difficult to resolve the mixed clusters from driver gas clusters. If we use an atomic gas that has a only one isotope, and has a high ionization potential, its clusters will not be detected, mixed cluster ions will be free from background ions of the driver gas. At the laser intensity ($10^{10} \text{ W cm}^{-2}$) available for the ionization of clusters, it is not possible to overcome the high ionization potential of Argon atoms (15.75 eV), and its ions will not contaminate the mass spectrum. It has one dominant isotope, making it the gas of our choice as a driver gas.

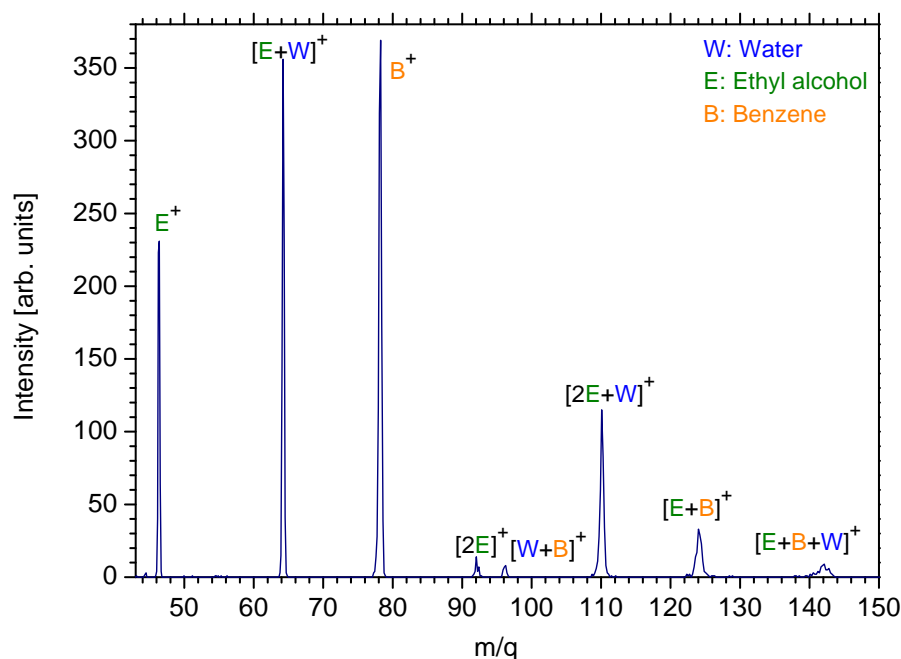


Figure 4.15: Mass spectrum of mixed clusters of Water vapor, Ethyl alcohol and Benzene.

For creating the mixed clusters vapor of Water molecules, Ethyl alcohol and Benzene is introduced in the high pressure Argon driver gas. Ionization is carried out at 355 nm laser pulse. The mass spectrum consist of several mixed clusters and ethyl alcohol cluster. A mass spectrum of mixed clusters with Ar driver is shown in Figure 4.15.

As a concluding remark of this chapter, the outcomes from the mass spectrometric investigation of hollow cathode sputtering source and pulsed nozzle source are discussed in detail. Hollow cathode sputtering source was used to generate a beam of carbon clusters and mixed clusters. Pulsed nozzle source was used to produce a beam of Xenon clusters, Ethyl alcohol clusters and mixed clusters of Ethyl alcohol, Water vapor and Benzene. The cluster ions are produced using 355 nm ionization.

Chapter 5

Multiply charged ion formation in MPI of Xenon clusters

In the previous chapter, the formation of singly charged cluster ions by MPI using 355 nm laser pulse has been discussed . Apart from 355 nm ionization, cluster ion formation using Nd:YAG 1064 nm pulse has been studied. When we compared the Xenon cluster ions mass spectrum under IR and UV irradiation, some interesting results are found. In this chapter, the difference in the ionization mechanism of Xenon clusters subjected to IR and UV irradiation are discussed.

5.1 IR irradiation: Multiple ionization

When 1064 nm radiation is employed for Xenon cluster ionization, the TOF mass spectrum shows singly ionized peaks of the monomer and the dimer, but, more interestingly, there are several multiply charged atomic ions (Xe^{q+} , $q = 1-5$). A sample mass spectrum with IR ionization at 3 bar stagnation pressure is shown in Figure 5.1.

The presence of clusters is vital for the production of multiply charged atomic ions. This was confirmed by obtaining a mass spectrum with the pulsed nozzle beam replaced by a low number density effusive beam of Xe gas (which is devoid of clusters). The mass spectrum in the case of effusive beam shows only Xe^+ peak, and no multiply charged ions.

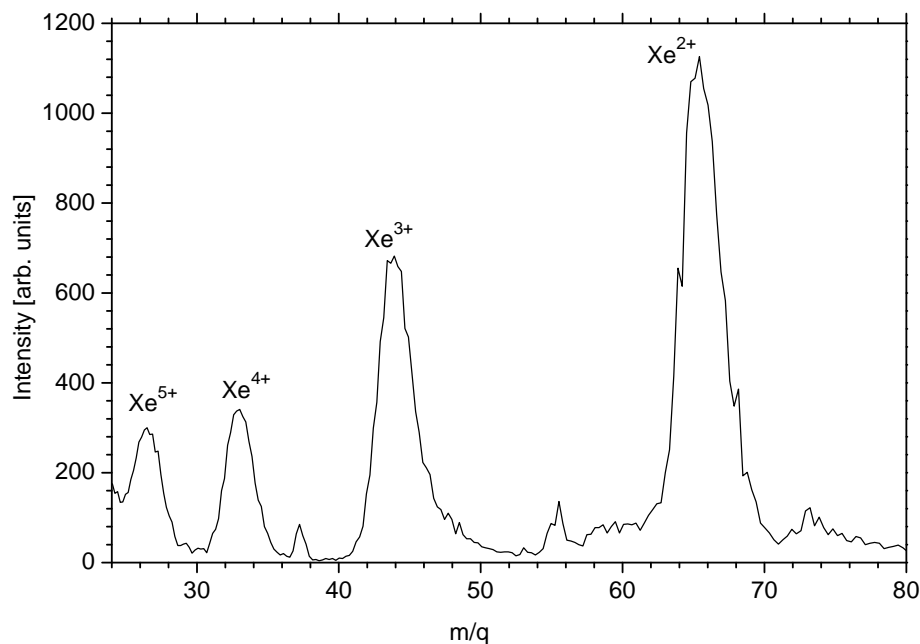


Figure 5.1: Mass spectrum of Xenon atomic ions from pulsed nozzle expansion at 3 bar stagnation pressure irradiated by 1064 nm laser pulses.

Similar reports of observation of multiply charged Xe ions from MPI of cluster beams exist in the literature for different wavelengths and laser intensities in the nanosecond regime [8–10]. Ionic states up to Xe^{13+} has been reported by Augst et al. [58] when Xe clusters are ionized using 1 ps focused laser pulses of wavelength 1053 nm ($\sim 10^{16} \text{W cm}^{-2}$). At higher laser intensities ($\sim 10^{17} \text{W cm}^{-2}$, 2 ps laser pulses), Ditmire et al. [61] have observed ionic charge states up to Xe^{29+} in the mass spectrum. At similar laser intensities, it has been found that the efficiency of the production of higher charge states of xenon atoms from clusters increases with compression of the time duration of laser pulses [4, 43, 62]. Ions with charge states upto Xe^{40+} and kinetic energy 1 MeV has been observed by Ditmire et al. in the ionization of Xe clusters irradiated by fs laser pulses of intensity $2 \times 10^{16} \text{W/cm}^2$ [6, 7]. Such ionization mechanisms and formation of multiply charged atomic ions from clusters have been discussed in the reports by Krainov et al. [42] and Saalman et al. [63].

Ionization Mechanisms

Ionization of Xe clusters occurs through MPI but MPI alone is inadequate for explaining the formation of multiply charged ions under IR irradiation at the intensity in the experiment, since the energy needed to ionize to the highest observed charge state, $5+$, is 53 eV [64]. Formation of multiply charged ions is explained on the basis of the electron re-collision model [65, 66] for IR wavelengths and high intensity nanosecond pulses. MPI of clusters results in formation of a positive ion residue to which the ejected electron remains quasi-bound. The quasi-bound electrons gain energy from the optical field through Inverse Bremsstrahlung (IB) mechanism and by re-collision with the residual ion. The collision of energetic electrons with clusters leads to the formation of multiply charged ions. The re-collision mechanism depends critically on the probability of the turn-around electron colliding with the cluster, so the larger the cluster size, the greater is the probability of electron re-collision leading to multiple ionization. *However, this theory can be substantiated only by indirect experimental inference for the neutral cluster size, as the actual neutral cluster size is very difficult to establish.*

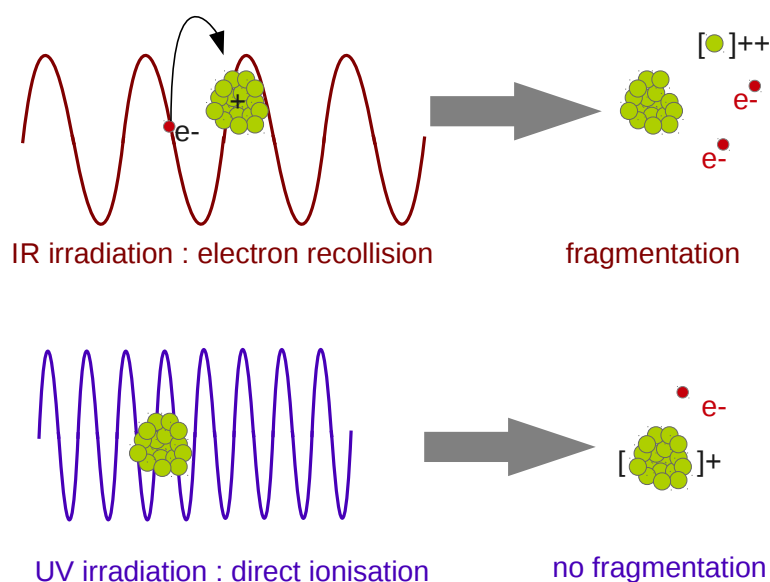


Figure 5.2: A schematic diagram showing the difference in the ionization mechanism of Xenon clusters exposed to IR and UV irradiation. Under IR, collisions of quasi-bound electrons with clusters lead to the production of multiply charged ions. Under UV, multiple ionization is almost suppressed.

A schematic diagram of Xe cluster ionization under IR and UV irradiation is shown in Figure 5.2.

In the nanosecond regime, the production of multiply charged atomic ions is based on the heating of quasi-free electrons by the optical field. In the majority of experiments, Xe cluster beam is generated by nozzle expansion and the size distribution of neutral clusters is inferred on the basis of Hagen's theory [13], which predicts that the average cluster size increases with the nozzle diameter and the stagnation pressure.

It was observed that the maximum kinetic energy of ions increases with increasing cluster size [6, 67]. A model has been developed to explain the large kinetic energies of the atomic ions thus formed [68]. An important point emerging from reports [8, 10] is that the production of multiply charged atomic ions increases with laser wavelength and neutral cluster size.

In view of the above, it is interesting to investigate how the yield of multiply charged ions depends on the cluster size. Furthermore, some relationship may also be expected between the kinetic energy and charge state carried by fragment ions as a function of the neutral cluster size as more electrons are quasi-bound to larger cluster surface [8]. For the investigation of the dependence of multiply charged ions and their kinematics on the neutral cluster size, mean cluster ion size is calculated from the mass spectra under UV irradiation (discussed in chapter 4). The mean cluster ion size determined from the mass spectrum under UV irradiation is treated as a proxy for neutral cluster size.

5.2 Characteristics of atomic ions resulting from MPI of clusters

For investigating the dependence of mean kinetic energy and mean charge state of fragment ions on cluster size, mass spectra of multiply charged Xe atomic ions are recorded under different stagnation pressures. These investigations reveal the dependence of distribution of fragment ions on cluster size.

Mean charge state of atomic ions

For quantifying the efficiency of multiple ionization, the yield (N_i) of each charge state (q_i) formed in the mass spectrum can be a useful parameter, provided a robust normalization method is available. However this is not the case, as even if the mass spectra are recorded for fixed parameters of Nd:YAG laser with the same number of shots, the flux of the cluster beam will not be constant for all the stagnation pressures. This prevents the proper normalization for the yield of multiply charged ions. The mean charge state, $\langle q \rangle$, of multiply charged atomic ions is estimated using equation (5.1).

$$\langle q \rangle = \sum_2^5 (q_i N_i) / \sum_2^5 (N_i) \quad (5.1)$$

Charge state 1 (monomer ions) is not included in the sum, since it can arise from the dissociative as well as the non-dissociative processes.

Mean kinetic energy of fragment ions

The Coulomb explosion of a multiply charged cluster ion leads the formation of atomic ions. The fragment ions with forward velocity (towards the detector) will arrive earlier at detector than the fragment ions with initial velocity away from the detector. The spread in the TOF profile due to the initial kinetic energy of ions can be used to calculate the mean kinetic energy of fragments. It is often the case, that a given ion may be formed by fragmentation of a variety of precursors. In such a situation, the TOF line shape corresponding to each fragmentation channel will be different. However, the individual line shapes will be symmetric about the same mean value, and the variance of the TOF profile will be the weighted average of the individual variances. The prescription for determining mean KE $\langle K \rangle$ following von Busch [69] is,

$$\langle K \rangle = \frac{3}{2m} q^2 E^2 \sigma^2 \quad (5.2)$$

where σ^2 is the variance of the TOF peak of mass m , charge q and E is the

electric field in the source region of the spectrometer.

Cluster size effect on kinetic energy and charge state of atomic ions

We now look into how the properties of the fragment ion distribution changes with the stagnation pressure, or in other words, with the mean cluster size. The variation of $\langle KE \rangle$ and $\langle q \rangle$ with the stagnation pressure will reveal that how the fragment ion distribution will be dependent on the cluster size in the pulsed nozzle beam. The variation of mean kinetic energy and mean charge state with mean cluster ion size is shown in Figure 5.3.

It is found that under IR irradiation, with fixed laser parameters, $\langle q \rangle$ and $\langle KE \rangle$ of each charge state increases with increasing stagnation pressure. This trend is consistent with the reports by Thomas et al. [43] and Das et al. [10], and with the model calculations of Islam et. al. [68], where the energy is parametrised against the

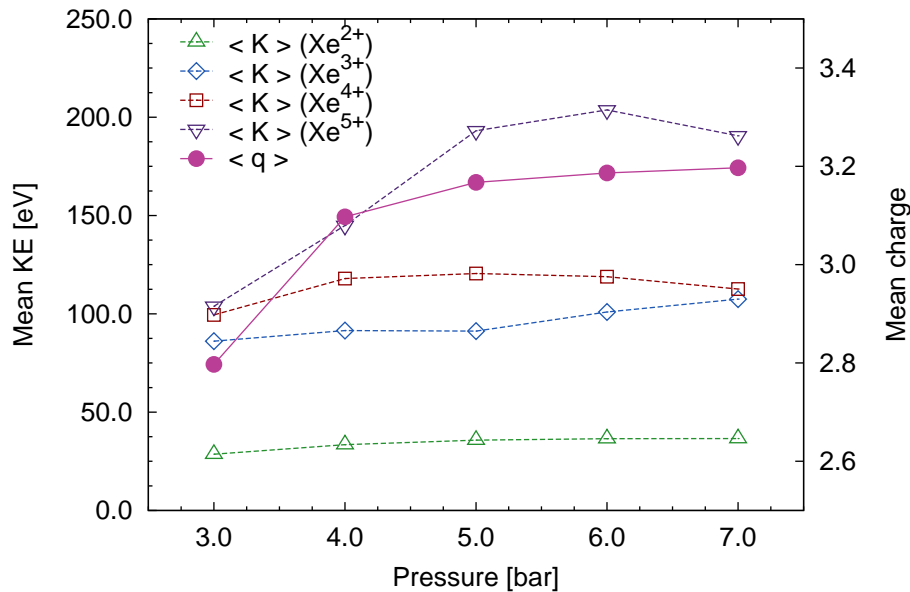


Figure 5.3: Variation of mean kinetic energy and mean charge state of atomic ions under IR irradiation, as a function of stagnation pressure. Left axis, open polygons: variation in the mean kinetic energy of the atomic ions having different charge states as a function of the stagnation pressure for jet expansion. Right axis, filled circles: mean charge state of multiply-charged atomic ions, observed when the cluster beam is subjected to IR irradiation. Lines are guides to the eye.

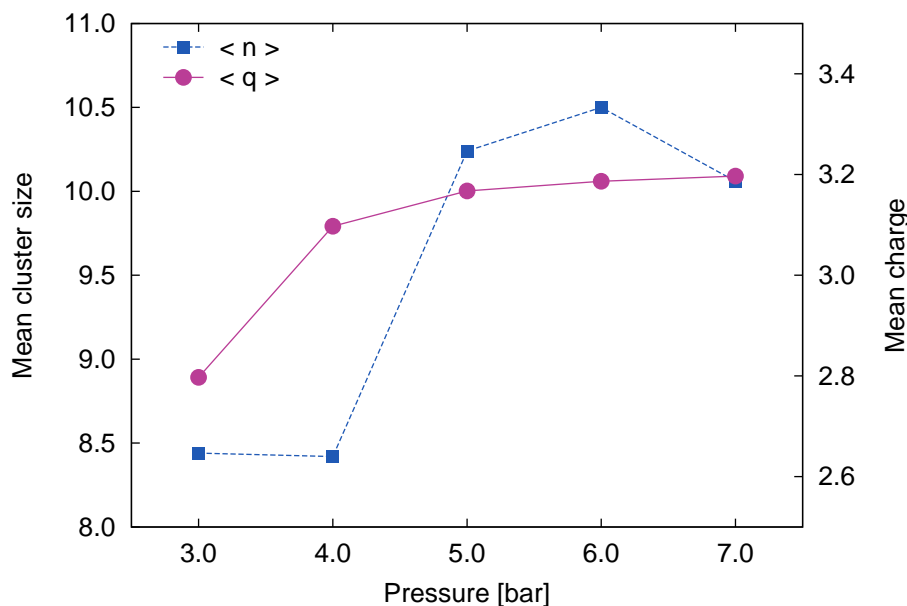


Figure 5.4: Variation of cluster ion size and atomic ion charge state from Xe clusters, with the stagnation pressure. Left axis, squares: the mean cluster ion size in the mass spectrum, under UV ionization of the of cluster beam. Right axis, circles: mean charge state of multiply-charged atomic ions, observed when the cluster beam is subjected to IR irradiation. Lines are guides to the eye.

cluster size, not the pressure. However, the values of the energies in various reports are difficult to compare with each other, as the techniques applied vary, and it is not clear whether the reported values are mean, most probable, or highest values. The kinetic energy of atomic ions shows an increasing trend with the cluster size in report by Islam et al. [68]. An increase in the mean kinetic energy of atomic ions with pressure or the size of the cluster is expected since with larger mass of the neutral cluster, the lighter atomic ions will carry away greater kinetic energy during coulomb explosion for the same charge sharing.

The variation of the mean cluster ion size (under UV) and mean charge state of atomic ions (under IR) with pressure is shown in Figure 5.4. A reasonable correlation is observed between the mean cluster ion size and the mean atomic ion charge. This correlation provide evidence for the validity of the electron re-collision model of multiple ionization.

As a concluding remark of this chapter, the ionization mechanisms of Xenon clusters under two different wavelength regime IR and UV have been studied. Un-

der IR irradiation, formation of multiply charged ions are observed while under UV irradiation singly charged heavy cluster ions are seen in the mass spectrum. The formation of multiply charged ions shows agreement with electron re-collision model. Ionization schemes of clusters are employed to investigate the effect of cluster size on the mean kinetic energy and mean charge state of fragment ions. It is found that the mean kinetic energy and mean charge state of fragment ions increases with the increasing cluster ions size.

Chapter 6

Summary and future prospects

6.1 Summary

To generate a beam of neutral clusters from solid, hollow cathode sputtering source and laser ablation source are developed. For producing carbon clusters, a rich environment of carbon soot is vital in hollow cathode sputtering source and laser ablation source. Optical emission spectroscopic study of carbon soot from these sources reveal the formation of carbon dimer.

Control over the formation of C_2 with the discharge current and Argon gas pressure in sputtering source is investigated using OES. It is found that C_2 yield increases with an increase in discharge current. An increase in gas pressure lead to an increase in three body collision thus cooling of ejecta improves and therefore T_{vib} preserves a decreasing trend with increase in gas pressure. It is found that the dominant process for C_2 production in the present source is the three body collision between carbon ejecta and Argon atoms. Emission spectroscopy of laser ablation source reveal the formation of C_2 and neutral C. Variation of C_2 intensity with delay, type of gas (Argon and N_2) and gas pulse duration have been studied. It is found that an increase in gas pulse duration lead to enhanced C_2 yield. Increase in gas pulse duration lead to increase number density of Argon atoms and thus cooling of C_2 gets improved.

Mass spectrometric study of sputtering source reveal the production of carbon clusters and mixed clusters of carbon and Argon. There are more complexities,

such as alignment of plume with gas and synchronization of three pulses (laser pulse used for ablation, gas pulse and ionizing pulse), involved in the laser ablation source. Due to any of these difficulties, we could not get TOF mass spectrum of carbon cluster ions using laser ablation source.

For generating clusters from gas, a pulsed nozzle source is developed. Using this source Xenon clusters, Ethyl alcohol clusters and mixed clusters of Water vapor, Ethyl alcohol and Benzene are produced. The effect of experimental parameters, such as delay, stagnation pressure and distance between nozzle and skimmer on cluster formation have been studied.

The multi-photon ionization (MPI) of Xenon clusters under IR irradiation and UV irradiation of an Nd:YAG laser with intensity $\sim 10^{10}$ W/cm² has been studied. Clusters are generated by a pulsed nozzle source. Clusters under IR irradiation lead to copious multiple ionization, giving atomic ions of charge states up to Xe⁵⁺. When clusters are ionized using UV irradiation, the ion yield is found to be nearly free of multiply charged ions, and comprises mainly of singly charged clusters ions. Xenon cluster ions up to size 70 are seen in the mass spectrum under UV irradiation. The mean cluster ion size observed in the mass spectrum is found to increase with the increasing stagnation pressure. The mean detected cluster ion size under UV irradiation is a reasonable proxy for the variation in the neutral cluster size distribution. As the effectiveness of the re-collision mechanism hinges on the size of the cluster, the observed positive trends in the mean cluster ion size, mean atomic ion charge state and the the mean kinetic energy of the atomic ion with the stagnation pressure provides support to the electron re-collision model for explaining multiple ionization.

6.2 Future prospects

The hollow cathode sputtering source can be used to generate beam of carbon clusters and pulsed nozzle source can be used to produce H₂O, NO_x, SO_x, CO₂ clusters. The collision of clusters with atoms, molecules as well as photo-ionization of different clusters can be studied using these sources.

The investigation of hetero-phase chemical reaction between the molecules adsorbed onto the surface of carbon clusters and exposed to UV photons can reveal the role of carbon clusters for the production of reaction product. For performing such experiments, a carbon cluster beam generated by sputtering source can be passed through a gas cell containing molecular vapor. The interaction between carbon cluster and molecule may lead to the adsorption of molecule on the surface of cluster resulting in the formation of mixed clusters. In the presence of UV irradiation, chemical reaction between the adsorbed molecules can be studied using TOF. The understanding of such complex reactions could be helpful to model the atmospheric reactions.

Bibliography

- [1] L. Belau, S. E. Wheeler, B. W. Ticknor, M. Ahmed, S. R. Leone, W. D. Allen, H. F. Schaefer and M. A. Duncan, *J. Am. Chem. Soc.* **129**, 10229–10243 (2007).
- [2] P. G. Reinhard and E. Suraud, *Introduction to cluster dynamics: Hardcover Edition; Wiley-VchVerlag Gmbh* (2004).
- [3] H. Pauly, *Atom, molecule and cluster beams part2: Hardcover Edition; Springer Berlin Heidelberg* (2000).
- [4] Y. L. Shao, T. Ditmire, J. W. G. Tisch, E. Springate, J. P. Marangos, and M. H. R. Hutchinson, *Phys. Rev. Lett.* **77**, 16 (1996).
- [5] A. McPherson, B. D. Thompson, A. B. Borisov, K. Boyer and C. K. Rhodes, *Nature* **370**, 631–634 (1994).
- [6] T. Ditmire, J. W. G. Tisch, E. Springate, M. B. Mason, N. Hay, R. A. Smith, J. Marangos, M. H. R. Hutchinson, *Nature* **54**, 386 (1997).
- [7] T. Ditmire, J. W. G. Tisch, E. Springate, M. B. Mason, N. Hay, J. P. Marangos, M. H. R. Hutchinson, *Phys. Rev. Lett.* **78**, 2732 (1997).
- [8] X. Luo, H. Li, D. Niu, L. Wen, F. Liang, B. Wang, and X. Xiao, *Phys. Rev. A* **76**, 013201 (2005).
- [9] D. Niu, H. Li, F. Liang, X. Luo and L. Wen, *Appl. Phys. Lett.* **87**, 034103 (2005).

-
- [10] S. Das, P. M. Badani, P. Sharma and R. K. Vatsa, *Chem. Phys. Lett.* **552**, 13–19 (2012).
- [11] K. Nagaya, H. Iwayama, H. Murakami, M. Yao, H. Fukuzawa, K. Motomura, K. Ueda, N. Saito, L. Foucar, M. Nagasono, A. Higashiya, M. Yabashi, T. Ishikawa, H. Kimura, H. Ohashi, *Journal of Electron Spectroscopy and Related Phenomena* **181**, 125–128 (2010).
- [12] H. Wabnitz, L. Bittner, A. R. B. de Castro, R. Dohrmann, P. Gurtler, T. Laarmann, W. Laasch, J. Schulz, A. Swiderski, K. von Haefen, T. Moller, B. Faatz, A. Fateev, J. Feldhaus, C. Gerth, U. Hahn, E. Saldin, E. Schneidmiller, K. Sytchev, K. Tiedtke, R. Treusch M. Yurkovk, *Nature* **420**, 482–485 (2002).
- [13] O. F. Hagen and W. Obert, *J. Chem. Phys.* **56**, 1793 (1972).
- [14] P. Fayet and L. Woste, *Surf. Sci.* **156**, 134 (1985).
- [15] W. Begemann, S. Dreihöfer, K. H. Meiwes-Broer and H. O. Lutz, *Z. Phys. D* **3**, 183 (1986).
- [16] T. F. Maguera, D. E. David and J. Michel, *J. Chem. Soc. Faraday Trans.* **86**, 2427 (1992).
- [17] A. C. Xenoulis, P. Trouposkiadis, C. Papastaikoudis, A. A. Katsanos and A. Clouvas, *Nanostructured Materials* **7**, 473 (1996).
- [18] S. Ahmad, *Eur. Phys. J. D* **18**, 309–318 (2002).
- [19] G. K. Wehner, *Adv. Electron. Electron Phys.* **7**, 258 (1955).
- [20] A. P. M. Baede, W. F. Jungman and J. Los, *Physica* **54**, 459 (1971).
- [21] P. Fayet and L. Woste, *Z. Phys. D.* **3**, 177 (1986).
- [22] D. M. Lindsay, F. Meyer and W. Harbich, *Z. Phys. D* **12**, 15 (1989).
- [23] S. A. Janjua, M. Ahmad, S. Khan, R. Khalid, A. Aleem and S. Ahmad, *J. Phys. D: Appl. Phys.* **40**, 1416–1421 (2007).

-
- [24] R. S. Pessoa, G. Murakami, G. Petraconi, H. S. Maciel, I. C. Oliveira, and K. G. Grigorov, *Braz. J. Phys.* **36**, 332 (2006).
- [25] A. C. Xenoulis, G. Doukellis, P. Tsouris, A. Karydas, C. Potiriadis, A. A. Katsanos and Th. Tsakalakos, *Vacuum* **51**, 357 (1998).
- [26] S. Ahmad, *Eur. Phys. J. D* **15**, 349–354 (2001).
- [27] L. P. Levine, J. F. Ready and E. Bernal, *J. Quantum Electron.* **4**, 18 (1968).
- [28] J. F. Friichtenicht, *Rev. Sci. Instrum.* **45**, 51 (1974).
- [29] J. C. Miller, *Laser ablation*, Springer, Berlin (1994).
- [30] D. J. Elliot, *Ultraviolet laser technology and applications*, Academic press-New York (1995).
- [31] H. W. Kroto, J. R. Heath, S. C. O'Brien, R. F. Curl, R. E. Smalley, *Nature* **318**, 162 (1985).
- [32] W. A. de Heer and P. Milani, *Z. Phys. D* **20**, 437–439 (1991).
- [33] M. A. Duncan, *Rev. Sci. Instrum.* **83**, 041101 (2012).
- [34] E. A. Rohlfing, D. M. Cox and A. Kaldor, *J. Chem. Phys.* **81**, 3322 (1984).
- [35] S. Maruyama, L. R. Anderson and R. E. Smalley, *Rev. Sci. Instrum.* **61**, 3686 (1990).
- [36] T. G. Dietz, M. A. Duncan, D. E. Powers, and R. E. Smalley, *J. Chem. Phys.* **74**, 6511 (1981).
- [37] H. Murphy and D. Miller, *J. Phys. Chem.* **88**, 4474 (1984).
- [38] E. W. Becker, K. Bier and W. Henkes, *Z. Phys.* **146**, 333 (1956)
- [39] O. F. Hagen, *Rev. Sci. Instrum.* **63**, 2374 (1992).
- [40] M. Lezius, S. Dobosz, D. Normand and M. Schmidt, *Phys. Rev. Lett.* **80**, 261 (1998).

-
- [41] A. V. Malakhovskii, *J. Phys. D* **33**, 556–563 (2000).
- [42] V. P. Krainov and M. B. Smirnov, *Physics Reports* **370**, 237–331 (2002).
- [43] H. Thomas, A. Helal, K. Hoffmann, N. Kandadai, J. Keto, J. Andreasson, B. Iwan, M. Seibert, N. Timneanu, J. Hajdu, M. Adolph, T. Gorkhover, D. Rupp, S. Schorb, T. Moller, G. Doumy, L. F. DiMauro, M. Hoener, B. Murphy, N. Berrah, M. Messerschmidt, J. Bozek, C. Bostedt, and T. Ditmire, *Phys. Rev. Lett.* **108**, 133401 (2012).
- [44] G. Chen, B. Kim, B. Ahn, and D. Eon Kim, *J. App. Phys.* **106**, 053507 (2009).
- [45] R. A. Smith, T. Ditmire and J. W. G. Tisch, *Rev Sci Instrum* (1998), **69**, 3798–3804.
- [46] O. F. Hagen, *Surf. Sci.* **106**, 101 (1981).
- [47] T. Gough, D. Knight and G. Scoles, *Chem. Phys. Lett.* **97**, 155 (1983).
- [48] S. Leutwyler, *J. Chem. Phys.* **81**, 5480 (1984).
- [49] C. P. Schulz, R. Haugstatter, H. U. Tittes and I. V. Hertel, *Z. Phys. D* **10**, 279–290 (1988).
- [50] W. Swan, *Transactions of the Royal Society of Edinburgh* **21**, 411–430 (1857).
- [51] R. W. P. McWhirter, *Spectral intensities, Plasma Diagnostic Technique*, R.H. Huddleston, S.L. Leonard (Eds.), Academic Press, New York (1965).
- [52] G. Herzberg. *Spectra of Diatomic Molecules (Molecular Spectra and Molecular Structure)–Vol.1*. New York: Van Nostrand, 2nd ed (1950).
- [53] W. C. Wiley and I. H. McLaren, *Rev. Sci. Instrum.* **26**, 1150–1156 (1955).
- [54] J. L. Wiza, *Nuclear Instrum. and Methods* **162**, 587–601 (1979).
- [55] G. S. Voronov and N. B. Delone, *Soviet Phys. JETP Letters* **1**, 66 (1965).
- [56] S. L. Chin, *Phys. Rev. A* **4**, 992–996 (1971).

- [57] L.V. Keldysh, Sov. Phys. JETP **20**, 1307 (1965).
- [58] S. Augst, D. Strickland, D. D. Meyerhofer, S. L. Chin and H. Eberly, Phys. Rev. Lett. **63**, 2212 (1989).
- [59] S. Das, P. Sharma and R. K. Vatsa, J. Chem. Sci. **121**, 965–972(2009).
- [60] I. S. Gilmore and M. P. Seah, Int. J. Mass Spec. **202**, 217 (2002).
- [61] T. Ditmire, P. K. Patel, R. A. Smith, J. S. Wark, S. J. Rose, D. Milathianaki, R. S. Marjoribanks and M. H. R. Hutchinson, J. Phys. B **31**, 2825–2831 (1998).
- [62] T. Ditmire, T. Donnelly, A. M. Rubenchik, R. W. Falcone and M. D. Perry, Phys. Rev A **53**, 3379–3402 (1996).
- [63] U. Saalman, Ch. Siedschlag and J. M. Rost, J. Phys. B **39**, 39–77 (2006).
- [64] L. A. LaJohn, P. A. Christiansen, R. B. Ross, T. Atashroo, and W. C. Ermler, J. Chem. Phys. **87**, 2812 (1987).
- [65] K. C. Kulander, K. J. Schafer and J. L. Krause, Laser Physics **3**, 359-364 (1993).
- [66] W. Wang, H. Li, D. Niu, L. Wen and N. Zhang, Chem. Phys. **352**, 111 (2008).
- [67] E. Springate, N. Hay, J. W. G. Tisch, M. B. Mason, T. Ditmire, J. P. Marangos and M. H. R. Hutchinson, Phys. Rev. A **61**, 063201 (2000).
- [68] Md. R. Islam, U. Saalman and J. M. Rost, Phys. Rev. A **73**, 041201 (2006).
- [69] F von Busch, J. Phys. B **34**, 431 (2001).